PAPER

MeV dark matter with MeV dark photons in Abelian kinetic mixing theories

Journal of Cosmology and Astroparticle Physics
An IOP and SISSA journal

MeV dark matter with MeV dark photons in Abelian kinetic mixing theories

Federico Compagnin,[a] **Stefano Profumo**[b] **and Nicolao Fornengo**[a,c]

[a]Dipartimento di Fisica, Università di Torino,
Via Pietro Giuria, 1, Torino 10125, Italy
[b]Department of Physics and Santa Cruz Institute for Particle Physics,
University of California,
Santa Cruz, CA 95064, U.S.A.
[c]Istituto Nazionale di Fisica Nucleare,
Torino, Italy

E-mail: federico.compagni@edu.unito.it, profumo@ucsc.edu,
nicolao.fornengo@unito.it

Received December 2, 2022
Accepted February 23, 2023
Published March 31, 2023

Abstract. We consider the cosmology and phenomenology of a dark photon portal to a simple dark sector consisting of a single, light, fermionic dark matter particle species with mass in the MeV range. We entertain three possible kinetic mixing structures of a new Abelian gauge group $U(1)_{dark}$ with the visible sector through $U(1)_{e.m.}$, $U(1)_Y$ and $T[SU(2)_L]$. We assume the dark photon to be massive and around the MeV scale, thus close to the mass scale of the dark matter candidate. We compute the dark matter relic density via freeze-out and freeze-in, entertaining the additional possibility of a late inflationary period that could dilute the dark matter yield of heavy candidates, and (ii) additional production modes, for models with under-abundant thermal production. We explore the parameter space compatible with a variety of experimental and astrophysical bounds, and discuss prospects for discovery with new CMB probes and MeV gamma-ray telescopes.

Keywords: dark matter theory, particle physics - cosmology connection

ArXiv ePrint: 2211.13825

https://doi.org/10.1088/1475-7516/2023/03/061

JCAP03(2023)061

Contents

JCAP03(2023)061

1 Introduction

The presence of dark matter (DM) has been established in numerous ways with cosmological and astrophysical observations throughout the past eighty years; it is now commonly agreed upon that the DM contributes around 24% of the Universe critical density at late times [1]. It is additionally agreed upon that this DM does not fit in the Standard Model (SM) of particle physics [2], and that it consists of a new particle species (or some heavy composite or compact object) [3].

The origin and production modes of the cosmological DM remain as mysterious as its particle nature. However, one paradigm has gained significant traction: that the DM consists of a *thermal relic*. In the thermal relic paradigm at early times the DM was in thermal equilibrium with the hot primordial plasma, where it interacted with other particles; upon "freezing out" of thermal equilibrium, while possibly non-relativistic, the DM would then free-stream and eventually collapse in the halos observed in the late universe, triggering the formation of structure in the universe. Such cold dark matter (CDM) paradigm is able to reproduce statistical properties of the large scale structure (LSS) of the Universe, and predicts

galaxy formations patterns consistent with observation [4]. A prototypical CDM candidate is a weakly interacting (being able to decouple with the measured relic abundance) massive (hence non-relativistic at the moment of decoupling) particle, or WIMP [5]. While the search for WIMPs via direct and indirect detection has produced no conclusive positive results, the possibility that the DM interact with the visible, Standard Model (SM) sector via some "portal" remains extremely well motivated [6–8].

Here we consider a "portal" to a minimal dark sector, consisting of a Dirac fermion DM candidate, blind to all known interactions leaving aside gravity, but charged under a new "dark" force, whose quantized nature is represented by a "Dark Photon" (DP) [9]. The latter is (weakly) coupled to charges in the SM, via kinetic mixing. Here, we will consider the following three possible kinetic mixing structures: $\mathrm{U}(1)_{\mathrm{dark}} \times \mathrm{U}(1)_{\mathrm{e.m.}}$, $\mathrm{U}(1)_{\mathrm{dark}} \times \mathrm{U}(1)_{\mathrm{Y}}$ and $\mathrm{U}(1)_{\mathrm{dark}} \times \mathrm{T}[\mathrm{SU}(2)_{\mathrm{L}}]$ mixing (where "T" stands for "maximal torus" of a given group).

The structure of our study is as follows. In the following section 2 we present our choice of kinetic mixing theories, describe their structure, and derive all couplings needed. This is explicitly done by rotating back the initial Lagrangian to the mass eigenstates where the kinetic terms are diagonal. The guiding idea is to introduce the minimum number of extra gauge bosons, in this case only one, the DP; for this additional gauge boson to interact with SM fields, one can only couple it with another neutral gauge boson within the SM, hence our choice of using the electromagnetic field A_μ, the hypercharge field B_μ and the $\mathrm{SU}(2)_{\mathrm{L}}$ — Cartan subalgebra generator W^3_μ.

The following section 3 discusses DM production from the primordial plasma: DPs are unstable particles and as such they may or may not be present at the beginning of DM production depending on whether they are still in equilibrium or have already decoupled and decayed. Here, we discuss these possibilities in detail, and find that the presence of DPs plays an important role in the solution to the relevant Boltzmann equations in the two production mechanisms discussed in the next section. We outline there the region where one may not assume $n_{A'} \neq 0$ at the moment of ignition of DM production ($n_{A'}$ being the number density of the DP).

Section 3 entertains two "thermal" DM production mechanisms, freeze-out and freeze-in, for DM candidates of mass 10 MeV and 100 MeV. We derive contour plots outlining the theory parameters combinations that yield the right amount of DM, and the regions where, for the 100 MeV candidate, a late-time inflationary period dilutes the standard DM abundance and opens up otherwise excluded parameter space. Finally we consider the freeze-in mechanism, where the DM is produced out of equilibrium starting from a null initial population. In this paradigm, DM is a "feebly" interacting massive particle (FIMP), for it is required not to reach thermal equilibrium throughout the entire thermal history of the early Universe [10–13]. In this case, the presence of DPs in the thermal bath will play a critical role in shaping the open parameter space and the ensuing observational and experimental bounds. In fact, when DPs are absent at early times, the only channel left for DM production is an s-wave process with DP exchange between SM particles and DM. In this case, the relevant interactions scale as $\Gamma \sim \left(g^{\mathrm{DP}}_{\mathrm{DM}}\right)^2 \left(g^{\mathrm{DP}}_{\mathrm{SM}}\right)^2 T$, while the Hubble rate $H \sim T^2/M_P$, where M_P is Planck's mass, meaning that the leading contributes are those of lower temperatures, i.e. DM will be independent from UV a priori unknown physics.

In section 4 we briefly review direct and indirect DM searches, as well as constraints on DM from CMB measurements in light of upcoming experiments such as NA64^{++}, the MeV telescope GECCO and the Simons Array. The final section 5 concludes.

We collect relevant analytical results in the appendices.

JCAP03(2023)061

2 The dark photon

In this section, we present a concise description of three different channels that may lead to the production of a new massive gauge boson that kinetically mixes with an Abelian SM gauge group. In particular, we give the terms one needs to add to the SM Lagrangian to obtain the operators stemming from the DP mixing.

2.1 Kinetic mixing theories

Kinetic mixing is a well-known mechanism to introduce DPs as portals between the SM and a dark sector assumed to contain the DM candidate. Here we explicitly derive all the needed couplings between the DS and the SM starting from the Lagrangian density where the mixing is explicit. Moreover, we address some of the differences between the theories presented in the next section, where phenomenological predictions will be made.

We start by looking at a $\mathrm{U}(1)_{\mathrm{e.m.}} \times \mathrm{U}(1)_{\mathrm{dark}}$ theory. The Lagrangian density under consideration is

$$\mathcal{L} = -\frac{1}{4}\tilde{F}_{\mu\nu}\tilde{F}^{\mu\nu} - \frac{1}{4}\tilde{F}'_{\mu\nu}\tilde{F}'^{\mu\nu} - \frac{\varepsilon}{2}\tilde{F}_{\mu\nu}\tilde{F}'^{\mu\nu} + eJ_\mu\tilde{A}^\mu + g_D J'_\mu \tilde{A}'^\mu, \tag{2.1}$$

where ε is the kinetic mixing parameter while e and g_D are the electric and "dark" charges. $J'_\mu = \bar{\chi}\gamma_\mu\chi$ is the "dark current", χ the DM candidate and J_μ is the usual electromagnetic current. $\tilde{F}_{\mu\nu}$ and $\tilde{F}'_{\mu\nu}$ are the field strengths respectively associated to the gauge fields $\tilde{A}_\mu$ and $\tilde{A}'_\mu$. Rotation into mass eigenstates is given in appendix B.

Another well motivated possibility, relevant to extending the model before the electroweak phase transition, is to make use of the other two neutral gauge bosons within the SM gauge group, namely the hypercharge boson B_μ and W^3_μ. We indicate the former as the $\mathrm{U}(1)_{\mathrm{Y}} \times \mathrm{U}(1)_{\mathrm{dark}}$ theory, obtained by rotating

$$\begin{aligned}\mathcal{L} = &-\frac{1}{4}B_{\mu\nu}B^{\mu\nu} - \frac{1}{4}W^3_{\mu\nu}W^{3,\mu\nu} - \frac{1}{4}a'_{\mu\nu}a'^{\mu\nu} - \frac{\varepsilon}{2}B_{\mu\nu}a'^{\mu\nu} \\ &+ (\mathcal{D}_\mu\Phi)^\dagger(\mathcal{D}^\mu\Phi) + \frac{1}{2}m^2_{a'}a'_\mu a'^\mu + i\bar{L}\not{\mathcal{D}}L + i\bar{\ell}_{\mathrm{R}}\not{\mathcal{D}}\ell_{\mathrm{R}} + i\bar{Q}\not{\mathcal{D}}Q \\ &+ i\bar{u}_{\mathrm{R}}\not{\mathcal{D}}u_{\mathrm{R}} + i\bar{d}_{\mathrm{R}}\not{\mathcal{D}}d_{\mathrm{R}} + i\bar{\chi}\not{\mathcal{D}}\chi\end{aligned} \tag{2.2}$$

into the mass eigenstates. Notice that in this case, we have to introduce a massive boson a'_μ which will be rotated into a new DP after symmetry breaking (see appendix C). In what follows, we will refer to the dark photon mass as $m_{A'}$, distinguishing it from $m_{a'}$ (see $m_{A'}(m_{a'})$ below). Also notice that the resulting $\hat{Z}_\mu$ boson inherits the kinetic mixing residual as a slight modification of the SM Z_μ due to its mass, see again appendix C for details.

The $\mathrm{T}[\mathrm{SU}(2)_{\mathrm{L}}] \times \mathrm{U}(1)_{\mathrm{dark}}$ case is obtained similarly by substituting the kinetic mixing term

$$\mathcal{L}_{\mathrm{mix}} = -\frac{\varepsilon}{2}W^3_{\mu\nu}a'^{\mu\nu} \tag{2.3}$$

in place of the B_μ-mixing in (2.2).

Before proceeding, we point out that all vertices containing a DP are of order $\mathcal{O}(\varepsilon)$; moreover in the two theories describing physics prior to the electroweak phase transition, the vertices comprising the $\hat{Z}_\mu$ boson correct SM interactions by terms of order $\mathcal{O}(\varepsilon^2)$. In these latter theories, neutrinos are the only "anomalous" particles interacting with DPs, with couplings of order $\mathcal{O}(\varepsilon\delta)$, where $\delta = (m_{A'}/m_Z)^2$.

JCAP03(2023)061

2.2 Thermal equilibrium

We now examine the question of whether dynamically tracking the dark photon abundance in computing the dark matter relic density is necessary. First, we point out that DP-SM interactions (such as $ff \longleftrightarrow A'A'$, $fA' \longleftrightarrow fA'$ and $\gamma f \longleftrightarrow A'f$) are greatly suppressed compared to dark sector processes. As a result, A' is in thermal equilibrium when the rates Γ for dark sector processes satisfy $\Gamma_{\chi\chi\to A'A'}/H > 1$ and $\Gamma_{A'A'\to\chi\chi}/H > 1$, or $\Gamma_{A'\chi\to A'\chi}/H > 1$ or both simultaneously. If one of the first two conditions is violated, the third one will prevent the decay, but when both are violated, then the particle is no longer in equilibrium. Notice also that we must require annihilation and production to be in equilibrium simultaneously: if one of the two is violated, then both are to be considered no longer available interactions to keep A' in equilibrium. Finally if the interactions are slower than the decay rate, then A' will decay, regardless of the equilibrium argument given above.

We computed the temperature at which A' starts decaying (T_D) and compared it with the temperatures of freeze-out $T_{\chi,\text{f.o.}}$ and freeze-in $T_{\chi,\text{f.i.}}$, whichever appropriate: if, for example, $T_D > T_{\chi,\text{f.o.}}$, DPs decouple before the beginning of DM production (through the freeze-out mechanism in this case) and hence they may be considered already decayed away. On the other hand if $T_D < T_{\chi,\text{f.o.}}$ then DPs have still to decouple, being therefore present at the moment DM starts being produced. We performed this analysis in the $(m_{A'}, \varepsilon^2)$ space, by checking the temperatures conditions outlined above for each parameter configuration, thus obtaining a parameter subspace where DP may still be present due to thermal equilibrium. We labelled the corresponding region in parameter space with $n_{A'} \neq 0$ and this region of parameter space the DP-DM Boltzmann equations must be solved as coupled differential equations. It's worth mentioning that if one was to simplify the coupled equations by assuming DP to have an equilibrium distribution, then their presence in the primordial plasma would have kept DM in equilibrium for a much longer time (due to "dark strong" interactions) hence producing no compatible freeze-out abundance. In the freeze-in scenario on the other hand, if one was to assume a non-negligible presence of DP during the initial thermal history, their interactions would have immediately overproduced DM leading again to wrong predictions.

We conclude this section illustrating the interplay of rates discussed above, normalized to the Hubble rate and to the DP decay rate as a function of temperature for a few choices of DM and DP masses. In figure 1 we consider DM masses $m_\chi = 10\,\text{MeV}$ and $m_\chi = 100\,\text{MeV}$, with $m_{A'} = 2\,\text{MeV}$, $m_{A'} = 10\,\text{MeV}$, $m_{A'} = 100\,\text{MeV}$ and $m_{A'} = 1\,\text{GeV}$ in the dark $\times$ electromagnetic theory. In the figure we show four ratios: $\Gamma_{\chi A'\to\chi A'}/H$, $\Gamma_{\chi A'\to\chi A'}/\Gamma_{A'}$, $\Gamma_{\chi\chi\to A'A'}/H$ and $\Gamma_{\chi\chi\to A'A'}/\Gamma_{A'}$. Notice that when the ratios Γ/H are greater than unity, interactions are rapid enough to keep the DP in equilibrium as long as in the meantime the condition $\Gamma/\Gamma_{A'} > 1$ is also satisfied. For example, in the $m_\chi = 100\,\text{MeV}$ and $m_{A'} = 1\,\text{GeV}$ section, even though A' could be in equilibrium thanks to elastic scatterings and inelastic interactions (continuous lines), the decay amplitude takes control and brings it to decay (dashed lines): leading interactions are always the ones we refer to, hence the dashed interactions "decouple" at higher temperatures i.e. a little sooner in the thermal history of the plasma. More precisely in the considered case we see that the "decoupling" temperature is about 1 GeV while the DM decoupling temperature is $T \sim m_\chi/20 \sim 5\,\text{MeV}$; as a result, we are allowed to assume no DP is present at the moment of DM decoupling. Vice-versa, in the upper left plot, we see that the DM decouples at $T \sim 5 \times 10^{-4}\,\text{GeV}$, when the DPs are still present in the plasma. In this case, the DPs abundance must be tracked to compute the final DM abundance.

JCAP03(2023)061

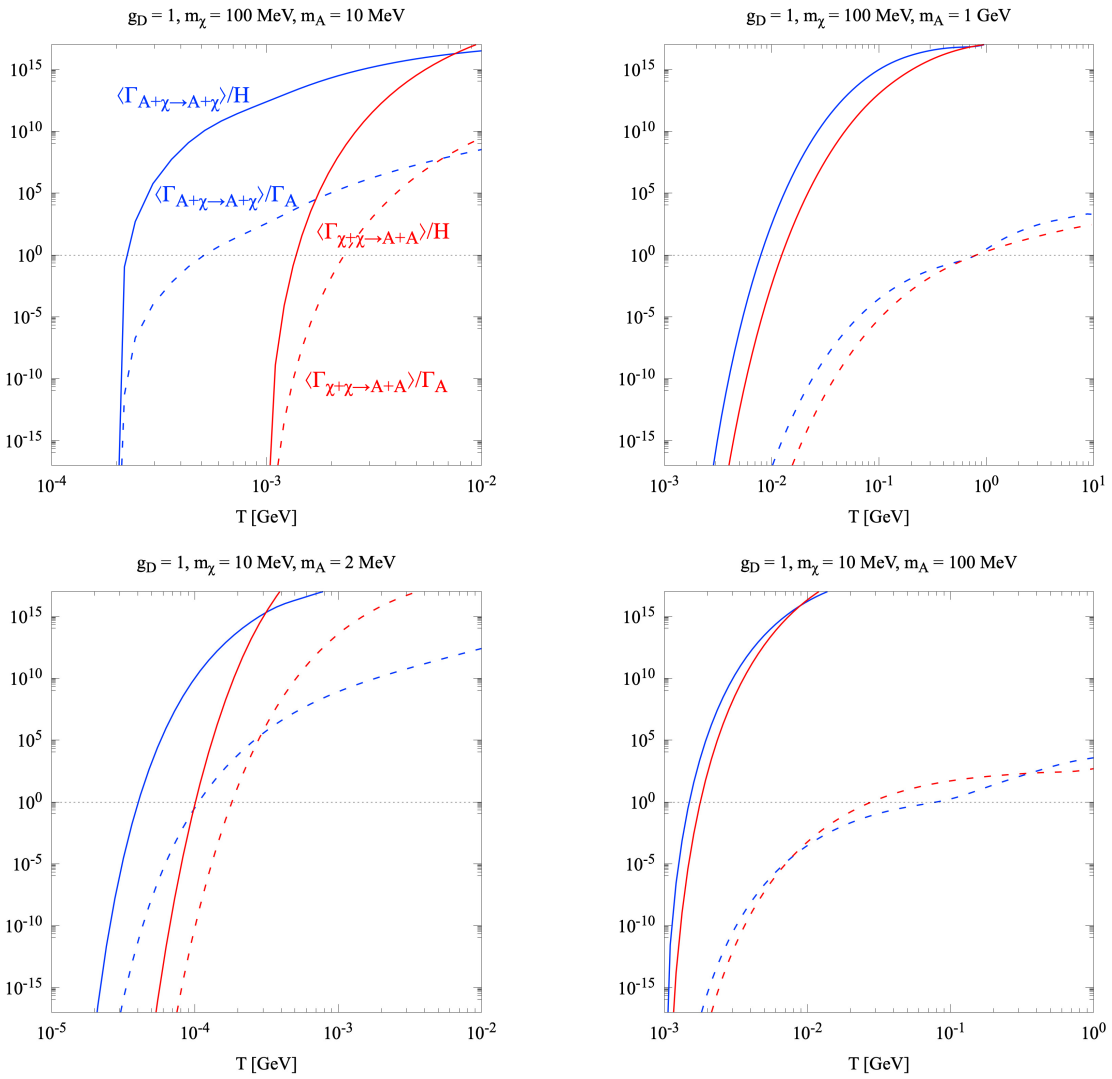

Figure 1. Considering the electromagnetic × dark theory we plot pair-production and elastic scattering rates, relative to the Hubble rate (solid lines) or to the A' boson decay rate (dashed lines), as a function of temperature for by $g_D = 1$, $m_\chi = 10\,\text{MeV}$ and $m_\chi = 100\,\text{MeV}$, for some representative values of $m_{A'}$. When the solid curves are below the horizontal dotted line, interactions are decoupled. When the dashed curves are below the horizontal dotted line, decay is fast enough to guarantee disappearance of the DP.

The freeze-out condition is shown in figure 2, where the light blue region indicates the subspace where $n_{A'} \ll 1$ cannot be assumed. In the case of freeze-in, instead, one must distinguish among the different scenarios, as they are relevant at different cosmological times, prior or subsequent to Electroweak Symmetry Breaking (EWSB); in the dark × electromagnetic theory, since DM may be produced from the very beginning of the thermal history of the universe, but the model is only valid up to EWSB, $T_{\chi,\text{f.i.}} \sim T_{\text{EWSB}}$ (which is very high) and we get that the presence of DP in this case can never be neglected. The last argument applies also to Y × dark and L × dark mixing theories, although in these we considered a generic post-inflationary high temperature $T \sim 200\,\text{GeV}$ (the precise value of the temperature is irrelevant, as we discuss below). Lastly, no matter which theory one considers, DP

JCAP03(2023)061

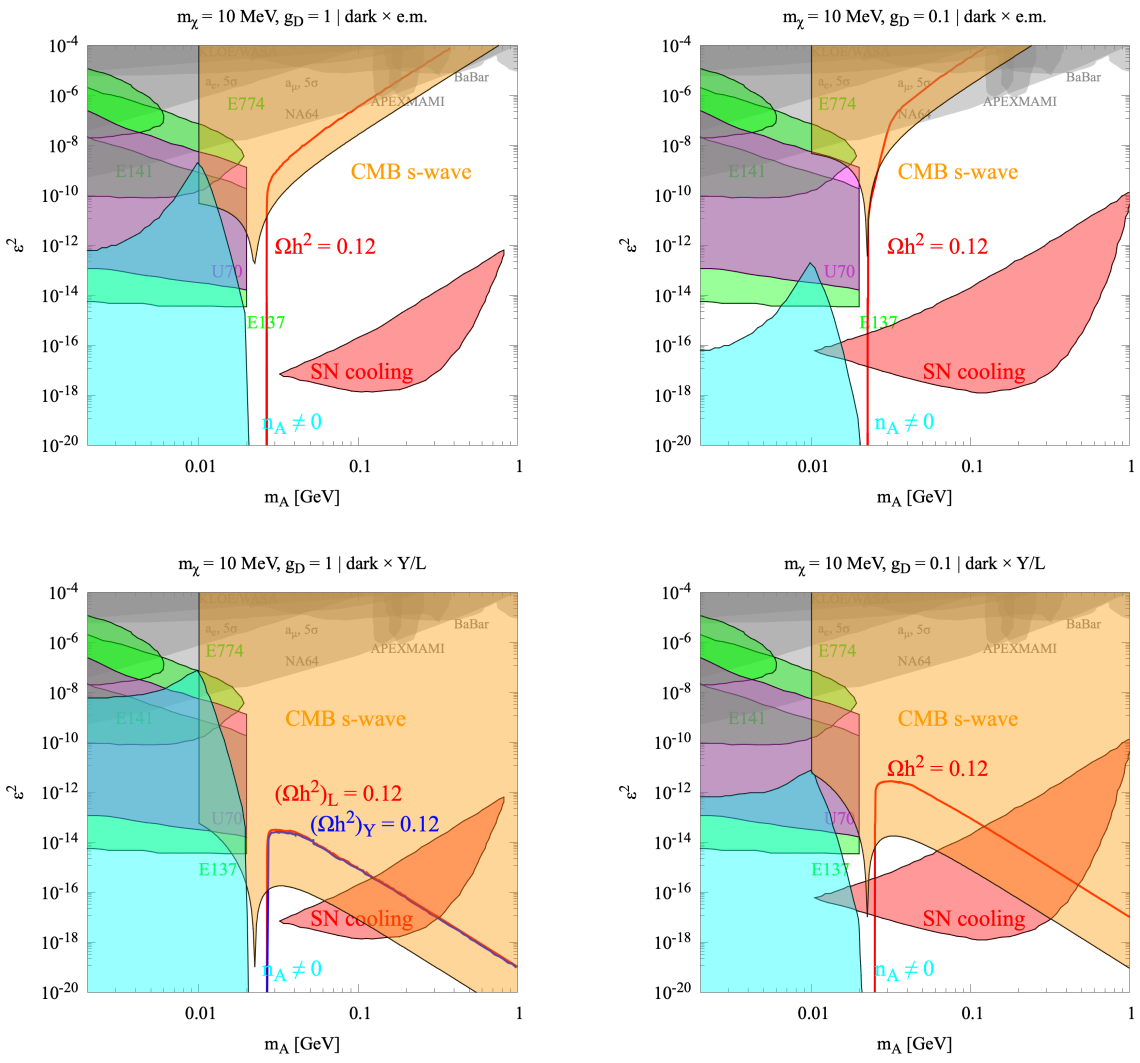

Figure 2. The relevant parameter space for the freeze-out production mechanism, for the theories dark × electromagnetic (above) and dark × Y/L (below). The plots show constraints from the E137, E141 and E774 beam dump experiments at SLAC (green coloured region) [16], the U70 beam dump experiment (purple) [17], the fixed target experiments MAMI [18] and APEX (brown) [19], the electron-positron collider experiments BaBar [20, 21] and KLOE (dark gray) [22]. Finally, constraints from the CMB assuming s-wave annihilation (orange) [23] and SN-cooling (red) [24]. The cyan region shows the parameters' configurations which may lead to a non-decoupled A' boson during freeze-out and hence depicting a region in parameter space where the approximation of negligible number density for A' is not valid. Red solid lines show the model's parameters where the DM relic density matches the cosmological value $\Omega h^2 = 0.12$; acceptable DM candidates are found where $A'A' \to \chi\chi$ interactions dominate and the model gets independent from ϵ^2. Finally, in the third frame we added a blue solid line, which shows that the region where $\Omega h^2 = 0.12$ in the dark × Y model is basically coincides with the region for the dark × Y/L model.

JCAP03(2023)061

processes $\chi\chi \longleftrightarrow A'A'$ (and $\chi A' \longleftrightarrow \chi A'$) are always very significant in the "strong dark" regime we consider below, one where the coupling $g_D \lesssim \mathcal{O}(1)$.

3 Production

We consider a standard homogeneous and isotropic FLRW universe, where the collisional Boltzmann equations take the form

$$\frac{dY_i}{dT} = -\frac{\tilde{g}}{sHT}\left(\frac{g_i}{(2\pi)^3}\int \frac{d^3p}{E}\mathcal{C}_{\text{inel}}[f_i;\dots]\right), \tag{3.1}$$

where $Y_i = n_i/s$ is the i-th species abundance, $s = (2\pi^2/45)g_{\star s}T^3$ is total entropy density [14], H the Hubble rate, g_i the degrees of freedom (d.o.f.) of i, $\mathcal{C}_{\text{inel}}$ the inelastic Collisional operator and f_i the phase space distribution function of i. $\tilde{g} = (1 + Td\log g_{\star s}/dT) \sim 1$ for $g_{\star s}$ only changes when a d.o.f. becomes non-relativistic in the plasma.

Integrating (3.1) we get the current value of $Y_{\chi,0}$ which we use for estimating the relic abundance

$$\Omega h^2 = \frac{m_\chi s_0}{\rho_{\text{crit},0}/h^2} Y_{\chi,0}(m_\chi, m_{A'}, \varepsilon, g_D), \tag{3.2}$$

known to be close to 0.12 from Planck data.

3.1 Freeze-out

Producing DM through a freeze-out scenario requires it to be in equilibrium with the plasma at the moment of decoupling, so we may take $Y_\chi = Y_\chi^{\text{eq}}$ with $n_\chi^{\text{eq}} = (g_i/2\pi^2)m_i^2 T K_2(m_i/T)$ [15], where K_2 is the modified Bessel function of the second kind.

In the electromagnetic kinetic mixing scenario we have the following system of equations:

$$\begin{aligned}
\frac{dY_\chi}{dT} &= -\frac{1}{sHT}\Big[(n_f^{\text{eq}})^2\langle\sigma v_{ff\to\chi\chi}\rangle - n_\chi^2\langle\sigma v_{\chi\chi\to ff}\rangle + n_{A'}^2\langle\sigma v_{A'A'\to\chi\chi}\rangle \\
&\quad - n_\chi^2\langle\sigma v_{\chi\chi\to A'A'}\rangle + 2n_{A'}\Gamma_{A'\to\chi\chi}\Big] \\
\frac{dY_{A'}}{dT} &= -\frac{1}{sHT}\Big[(n_f^{\text{eq}})^2\langle\sigma v_{ff\to A'A'}\rangle - n_{A'}^2\langle\sigma v_{A'A'\to ff}\rangle + n_\chi^2\langle\sigma v_{\chi\chi\to A'A'}\rangle \\
&\quad - n_{A'}^2\langle\sigma v_{A'A'\to\chi\chi}\rangle - n_{A'}\Gamma_{A'\to\chi\chi} + n_f^{\text{eq}}n_\gamma^{\text{eq}}\langle\sigma v_{f\gamma\to fA'}\rangle - n_f^{\text{eq}}n_{A'}\langle\sigma v_{fA'\to f\gamma}\rangle\Big]
\end{aligned} \tag{3.3}$$

whilst in the hypercharge and W^3-mixing theories more terms are needed to account for processes where $\hat{Z}$ participate to the interactions (see appendix C for its definition). On the other hand, as mentioned in the previous section, $\hat{Z}$ is quite heavy if compared to DP and its presence may be neglected in a first approximation. We thus take $n_{A'}$ to be zero at the moment of DM freeze-out, in such a way we are allowed to solve the first equation independently of the second one:

$$\frac{dY_\chi}{dT} = \frac{1}{HT}\langle\sigma v_{\text{ann, tot}}\rangle\left(Y_\chi^2 - Y_{\text{eq},\chi}^2\right) \overset{\text{cold relic}}{\sim} \frac{1}{HT}\langle\sigma v_{\text{ann, tot}}\rangle Y_\chi^2, \tag{3.4}$$

JCAP03(2023)061

where we take $Y_{\text{f.o.},\chi} \equiv Y_\chi(T_{\text{f.o.}}) = Y_{\text{eq},\chi}(T_{\text{f.o.}})\,(1+\delta)$ with $\delta = 1.5$. In this way, the present-day relic abundance can be computed as

$$Y_{\chi,0} = \frac{Y_{\text{f.o.},\chi}}{1 + \mathcal{I}\, Y_{\text{f.o.},\chi}}, \tag{3.5}$$

with

$$\mathcal{I} \equiv \sqrt{\frac{\pi}{45}} M_P \int_{T_0}^{T_{\text{f.o.}}} dT\, \frac{g_{\star s}}{\sqrt{g_\star}} \langle \sigma v_{\text{ann, tot}} \rangle. \tag{3.6}$$

We have the following situation for the three theories under consideration:

$$\begin{aligned}
\text{dark} \times \text{e.m.}: &\quad \langle \sigma v_{\text{ann, tot}} \rangle \sim \langle \sigma v_{\chi\chi \to e^+e^-} \rangle + \langle \sigma v_{\chi\chi \to A'A'} \rangle \\
\text{dark} \times \text{Y}: &\quad \langle \sigma v_{\text{ann, tot}} \rangle \sim \langle \sigma v_{\chi\chi \to e_L^+ e_L^-} \rangle + \langle \sigma v_{\chi\chi \to e_R^+ e_R^-} \rangle + \sum_{\ell = e,\,\mu,\,\tau} \langle \sigma v_{\chi\chi \to \nu_{\ell_{\text{L}}} \nu_{\ell_{\text{L}}}} \rangle + \langle \sigma v_{\chi\chi \to A'A'} \rangle \\
\text{dark} \times \text{L}: &\quad \langle \sigma v_{\text{ann, tot}} \rangle \sim \langle \sigma v_{\chi\chi \to e_L^+ e_L^-} \rangle + \langle \sigma v_{\chi\chi \to e_R^+ e_R^-} \rangle + \sum_{\ell = e,\,\mu,\,\tau} \langle \sigma v_{\chi\chi \to \nu_{\ell_{\text{L}}} \nu_{\ell_{\text{L}}}} \rangle + \langle \sigma v_{\chi\chi \to A'A'} \rangle\,.
\end{aligned}$$

Notice that we only considered $\mathcal{O}(\varepsilon)$ processes consisting of electron-positron pairs. This has been numerically checked and it turned out that the total contribution of particles heavier than electrons sums up to around 1% of the integral $\mathcal{I}$, and were neglected in what follows.

Finally, the theoretical abundance parameter Ωh^2 can be computed as (3.2).

3.1.1 10 MeV DM

We start by considering a $m_\chi = 10\,\text{MeV}$ DM candidate. Results are presented starting from figure 2 as contour plots of $\Omega h^2 = 0.12$.

The filled regions are constrained by experimental bounds, including beam dump experiments at SLAC such as E137 and E141, E774 at Fermilab [16], NA64 at CERN, beam dump U70 experiment [17], fixed target experiments like MAMI [18] and APEX [19], e^+e^- collider experiments such as BaBar [20, 21] and KLOE [22]. Finally, we show astrophysical constraints from CMB assuming s-wave annihilation [23] and SN-cooling [24]. The light blue region refers to the region where $n_{A'} \neq 0$ and DP are still in equilibrium after DM decoupled.

First, let us comment on how DM interactions play an important role in defining the correct value of the relic abundance. For simplicity we'll be referring our general discussion to the dark × electromagnetic theory, adjusting the argument whenever needed to include the other theories.

When $m_\chi \lesssim m_{A'}$, the leading interactions are $\chi\chi \to e^+e^- \sim e\varepsilon g_D$ and the weak scale is reached in the coupling constants product for the abundance to be produced correctly. On the other hand, when $m_\chi \gtrsim m_{A'}$ channels t and u open up, making the annihilation into two DPs $\chi\chi \to A'A' \sim g_D^2$ the leading interaction. In our g_D range, the latter is too strong to reach the weak scale, hence DM stays in equilibrium much longer than before, leading to its final relic abundance being extremely small due to Boltzmann suppression.

A very finely-tuned parameters configuration is obtained in the neighborhood of $m_\chi \sim m_{A'}$ in the $\varepsilon^2(m_{A'})$-plane: for dark × electromagnetic, $\varepsilon^2 \lesssim 10^{-14}$ when $(m_{A'} = 26.6\,\text{MeV}, g_D = 1)$, $(m_{A'} = 22.5\,\text{MeV}, g_D = 10^{-1})$ whilst for dark × Y, $\varepsilon^2 \lesssim 10^{-18}$ when $(m_{A'} = 21.6\,\text{MeV}, g_D = 1)$ and $\varepsilon^2 \lesssim 10^{-17}$ when $(m_{A'} = 22.1\,\text{MeV}, g_D = 10^{-1})$.

As mentioned in section 3, the difference between dark × Y and dark × L is of order $\mathcal{O}(\varepsilon^2)$: we therefore show, in the third plot in figure 2 both predictions, but in what follows we will make use only of dark × Y theory as representative of both.

JCAP03(2023)061

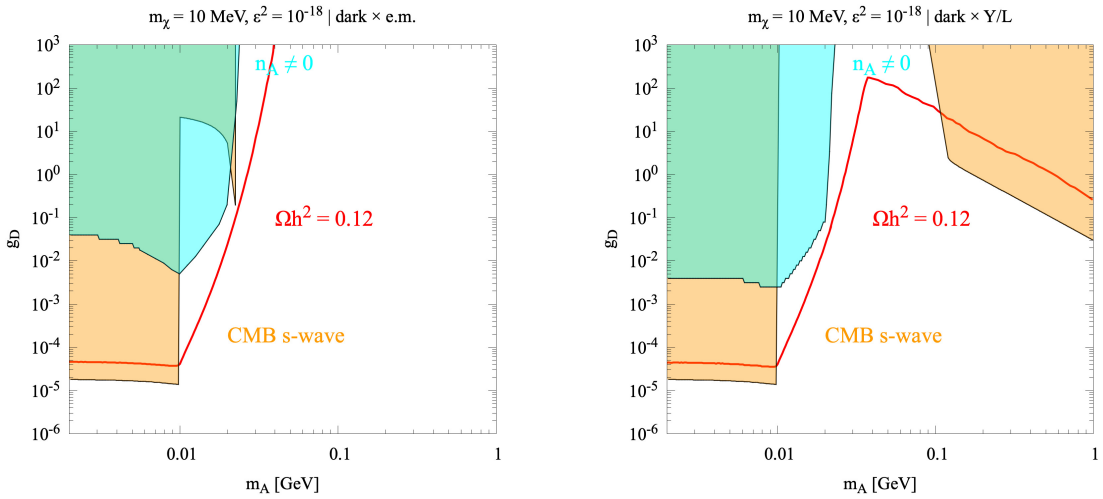

Figure 3. Parameter space for the freeze-out mechanism, for the dark × electromagnetic theory (left) and dark × Y (right) (which has similar results to the L kinetic mixing theory). The plots show the CMB constraints (orange) and the region where the abundance of A' is negligible (cyan); see figure 2 for detailed explanation. The red solid line shows the parameters configuration where the observed values of the relic abundance $\Omega h^2 = 0.12$ is matched.

Another interesting aspect of these results is the behaviour of $\Omega h^2 = 0.12$ upon changes in g_D: while on the right part of the plot the product $q_f e \varepsilon g_D$ decreases, requiring the DP to take up lighter and lighter masses, on the left side the singular behaviour moves slightly to the left, indicating an ε-independent configuration. This can clearly be seen in figure 3, where we specifically focus on that slice of parameter sub-space. When $m_\chi \gtrsim m_{A'}$ on-shell DPs production is the leading interaction for greater g_D, bringing the annihilation cross section close to threshold value from CMB s-wave. Notice that in this case, when considering the dark × Y theory, we get two regions where CMB bounds are effective: this may be understood looking at this $g_D(m_{A'})$ plane as the $\varepsilon^2 = 10^{-18}$ section of the previous $\varepsilon^2(m_{A'})$ plane for the same theory. Finally, the relic density requirement forces a $g_D \sim$ const for $m_{A'} \lesssim m_\chi$, interestingly already excluded by CMB bounds. However, for larger masses, the relic density forces larger values of g_D, in a region we indicate as "dark strong" interacting DM.

3.1.2 Inflated DM

Here we entertain the possibility that the dark matter candidate be heavier, $m_\chi = 100\,\text{MeV}$, and that a late entropy injection episode occurs between the dark matter freeze-out temperature and Big Bang Nucleosynthesis (BBN) so that a larger-than-expected thermal relic density can be reconciled with observations.

The freeze-out temperature for a $m_\chi = 100\,\text{MeV}$ Dirac fermion, which decouples as a cold relic is approximately given by $x_{\text{f.o.}} \sim 15 + 3\log(m_\chi/\text{GeV}) \sim 8$ hence $T_{\text{f.o.}} \sim 13\,\text{MeV}$. Here, we consider a period of "Late Inflation", by which we mean a model where an entropy dilution episode occurs at times close, but preceding, Big Bang Nucleosynthesis (BBN), i.e. $T_{\text{BBN}} \sim 1\,\text{MeV}$. Such episode would dilute the DM relic abundance, and offset its late-time asymptotic value.

As concrete example we consider the model outlined in ref. [25] which comprises a real scalar, coupled to fermions as well as self coupled through a suitable potential (bounded from

JCAP03(2023)061

below as a result of a $\mathbb{Z}_2$ symmetry)

$$\mathcal{L} = \frac{1}{2}\partial_\mu\phi\partial^\mu\phi - V[\phi] - \frac{1}{2}\mu_\chi\phi^2 + \sum_f y_f f\bar{f}\phi \tag{3.7}$$

Requiring the DM to have frozen-out before the late-time "inflationary period", by which we indicate the period when ϕ decays out of equilibrium increasing the total entropy density of the Universe, leads to a DM relic abundance which is diluted by a factor Δ which may be very large, depending on the couplings y_f. As a result, the thermal relic abundance is related to its value in absence of the ϕ decay by

$$(\Omega h^2)_{\text{after}} = \frac{(\Omega h^2)_{\text{before}}}{\Delta}. \tag{3.8}$$

For this to hold, however, one must ascertain that the DM species decouple *before* ϕ's decay, thus one needs to consider DM with mass at least $m_\chi \gtrsim 20\,\text{MeV}$; as a concrete example, here we pick $m_\chi = 100\,\text{MeV}$.

We show slices of the relevant parameter space in figures 4 and 5. The two top panels focus on the dark × electromagnetic case, while in the bottom panels we consider the dark × Y/L case. The plots show predictions for a DM candidate of $m_\chi = 100\,\text{MeV}$ in a standard cosmology ($\Delta = 1$, red continuous line) and for two dilution factors, $\Delta = 10^3$ (magenta) and $\Delta = 10^6$ (purple). Notice that the latter two open up new regions of parameter space as the DM yield must be over-abundance to get diluted into the right amount. In turn, this forces the interaction rates (in this region, dominantly $\chi\chi \to e^+e^-$) to be suppressed, with respect to the $\Delta = 1$ case, for the DM to decouple sooner from the primordial plasma and hence to get overproduced by the right amount that later gets diluted away.

In figure 5 we focus on a single value for ε, and continue to consider $m_\chi = 100\,\text{MeV}$. Here, even a small Δ allows to evade the CMB constraints, and opens up the parameter space at small dark photon masses $m_A \ll m_\chi$. For $m_A > m_\chi$ the non-trivial dependence of $g_D(m_{A'})$ sets in again. We conclude that as long as $T_{\text{f.o.}} > T_{\text{BBN}}$, dilution factors generically enable consideration of a significantly wider portion of the theory parameter space.

3.2 Freeze-in

Let's now turn to the freeze-in mechanism. Here one assumes the DM to be absent from the early Universe thermal bath, and DM production to result from out-of-equilibrium processes instead, with the DM remains permanently out of equilibrium. In this case, we define an "initial" temperature of freeze-in production to be the highest temperature compatible with our model, i.e. $T_{\text{f.i.}} = T_{\text{EWSB}}$ for the dark × electromagnetic model and a generic post-inflationary temperature, which we fix to $T_{\text{f.i.}} = 200\,\text{GeV}$ for the dark × Y/L models. Even though in principle one should consider new physics to uniquely determine such temperatures, we will argue below that the dependence on this $T_{\text{f.i.}}$ value is extremely suppressed and only extremely strong interactions may produce non-negligible production at high temperatures. In a nutshell though, it is sufficient to notice that relevant interactions are faster than the Hubble rate. As mentioned in the introduction, this happens when temperatures are low, from where we deduce that thermal freeze-in is an IR-dominated mechanism. For complete analytical expressions of interaction rates we refer the reader to appendix A.

Note that if we assumed DPs to be present during DM freeze-in, due to strong interactions $g_D \gg \varepsilon$, they would bring DM to equilibrium at least within the DS plasma, resulting

JCAP03(2023)061

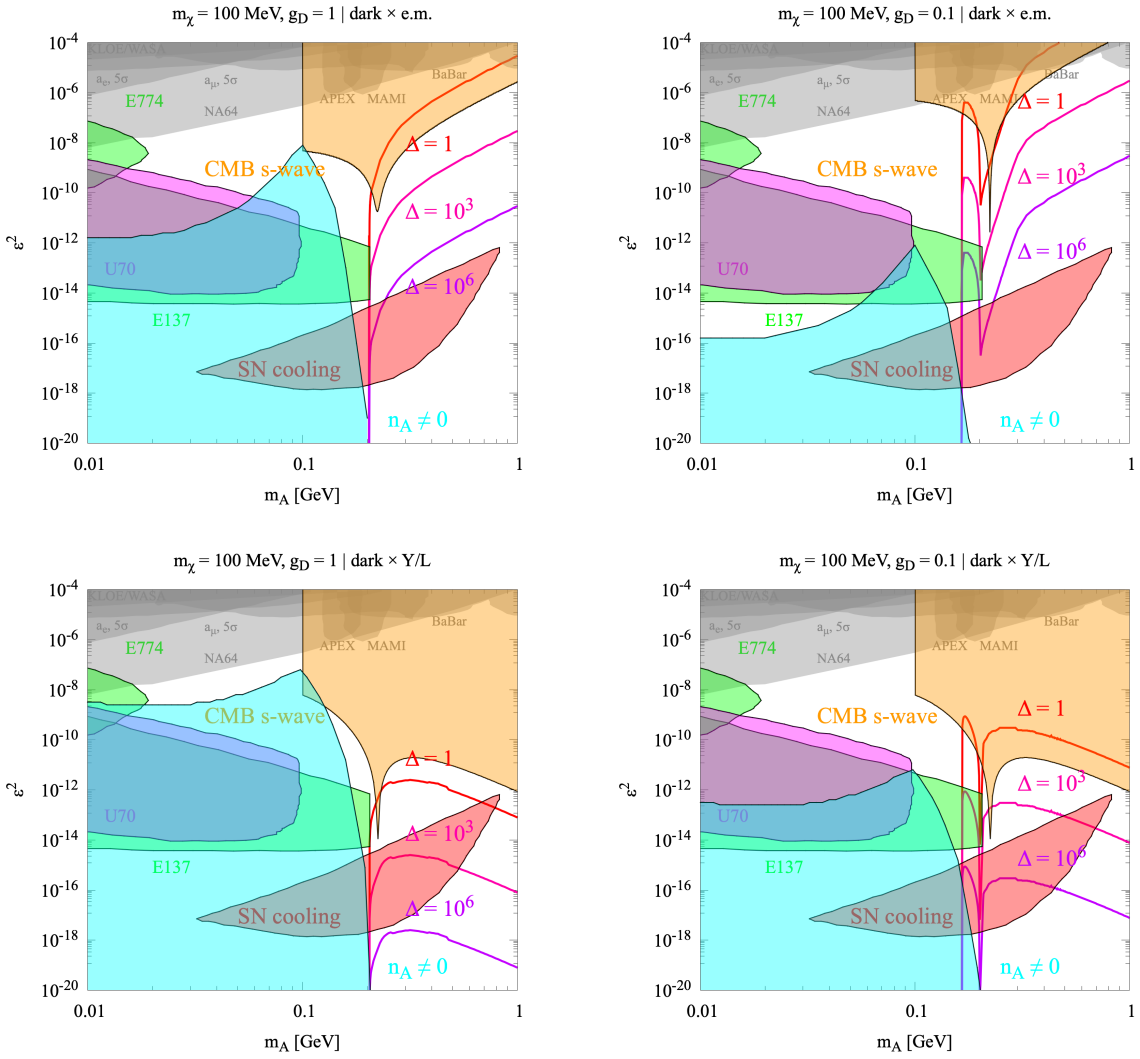

Figure 4. Results for the freeze-out mechanism with dilution, for the dark × electromagnetic (top panels) and dark × Y (bottom panels) models. The plots refer $m_\chi = 100\,\text{MeV}$. Experimental constraints are notes as in figure 2. The solid lines (red to purple) show the parameters configuration for which the relic abundance of DM matches the observational value $\Omega h^2 = 0.12$, for different dilution factors Δ.

in production via freeze-out as discussed above. Assuming then $n_{A'} = 0$, the Boltzmann equation for DM reads:

$$\frac{dY_\chi}{dT} \sim -\sqrt{\frac{\pi}{45}} M_P \frac{g_{\star s}}{\sqrt{g_\star}} Y^2_{\text{eq},f} \langle \sigma v_{\text{prod}} \rangle, \tag{3.9}$$

where

$$\text{dark} \times \text{e.m.}: \quad \langle \sigma v_{\text{prod}} \rangle \sim \langle \sigma v_{e^+e^- \to \chi\chi} \rangle \tag{3.10}$$

$$\text{dark} \times \text{Y}: \quad \langle \sigma v_{\text{prod}} \rangle \sim \langle \sigma v_{e_L^+ e_L^- \to \chi\chi} \rangle + \langle \sigma v_{e_R^+ e_R^- \to \chi\chi} \rangle + \sum_{\ell = e,\mu,\tau} \langle \sigma v_{\nu_{\ell_L} \nu_{\ell_L} \to \chi\chi} \rangle \tag{3.11}$$

$$\text{dark} \times \text{L}: \quad \langle \sigma v_{\text{prod}} \rangle \sim \langle \sigma v_{e_L^+ e_L^- \to \chi\chi} \rangle + \langle \sigma v_{e_R^+ e_R^- \to \chi\chi} \rangle + \sum_{\ell = e,\mu,\tau} \langle \sigma v_{\nu_{\ell_L} \nu_{\ell_L} \to \chi\chi} \rangle \,. \tag{3.12}$$

JCAP03(2023)061

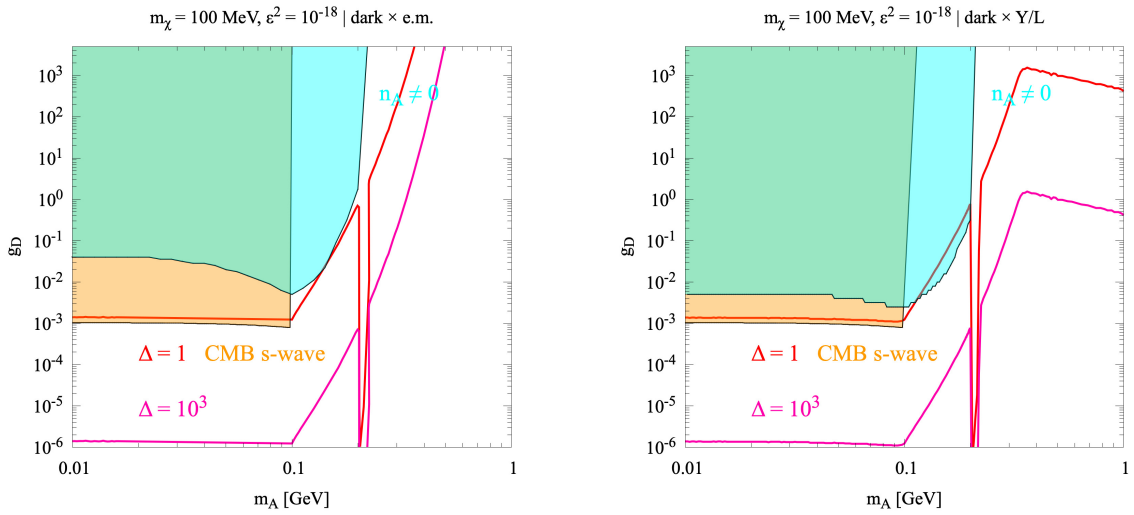

Figure 5. Freeze-out prediction for $m_\chi = 100\,\mathrm{MeV}$, in the dulution case. Orange regions are CMB s-wave constraints while light blue regions are configurations for which the A' abundance is not negligible (and therefore a complete solution of the evolution equations is required). Solid (red and magenta) lines show parameters configurations for which the DM abundances matches the observed value $\Omega h^2 = 0.12$, for two different values of the dilution parameter Δ.

Another possible complication arises in connection with the presence of light quarks participating in DM production (and hence dividing the integration domain into $(T_{\mathrm{EWSB}}, \Lambda_{\mathrm{QCD}})$ and $(\Lambda_{\mathrm{QCD}}, T_0)$); however, we find that the quark contribution, even after summing over all possible light degrees of freedom, is on the order of 1% of the total relic density. In fact, light quarks only contribute between $(T_{\mathrm{EWSB}}, \Lambda_{\mathrm{QCD}})$, i.e. when the high temperature suppression is still active. Electrons on the other hand contribute during the entire thermal history of the early Universe, resulting as the leading production initial states. Hadronic states contributions may come from light hadrons such as pions producing DM in the final state, but these would be inevitably strongly Boltzmann-suppressed due to the hadron masses. We note that an exception might consist of purely hadrophilic DM, where it has been shown pions can in fact give a substantial contribute in the case of a scalar mediator [26].

In figure 6 we analyze DM candidates with masses $m_\chi = 10\,\mathrm{MeV}$ (magenta lines) and $m_\chi = 100\,\mathrm{MeV}$ (violet lines) for coupling constants $g_D = 1$ and $g_D = 0.1$ in a normal freeze-in production, as well as in a situation where a more complex dark sector may be present (dashed lines). In particular, for the latter we assume that not all the DM contributing to Ωh^2 results from freeze-in, but only a fraction $\eta(\Omega h^2)_{\mathrm{tot}}$ of it. We find that values of $\eta \ll 1$ bring us far away from experimental sensitivities, which are already too weak to constraint a full thermal production mechanics, making non-entirely thermal mechanisms harder to verify considering only thermal signatures. The parameter η may also be used to quantify the overproduction that arises from the same freeze-in mechanics when considering stronger interactions — i.e. increasing values of ε^2. Taking the candidate $m_\chi = 100\,\mathrm{MeV}$ as an example, we coloured in purple the region where an overproduction of relic density is expected, due to greater values of coupling $\varepsilon e g_D$. Interestingly, these overproduced abundances are the only ones, up to now, compatible with experimental constraints such as SN cooling and collider searches. Finally, we bounded DM overproduction (OP) with a threshold value of η_{th} above which we found thermal equilibrium is reached during freeze-in production, leading DM to a freeze-out

JCAP03(2023)061

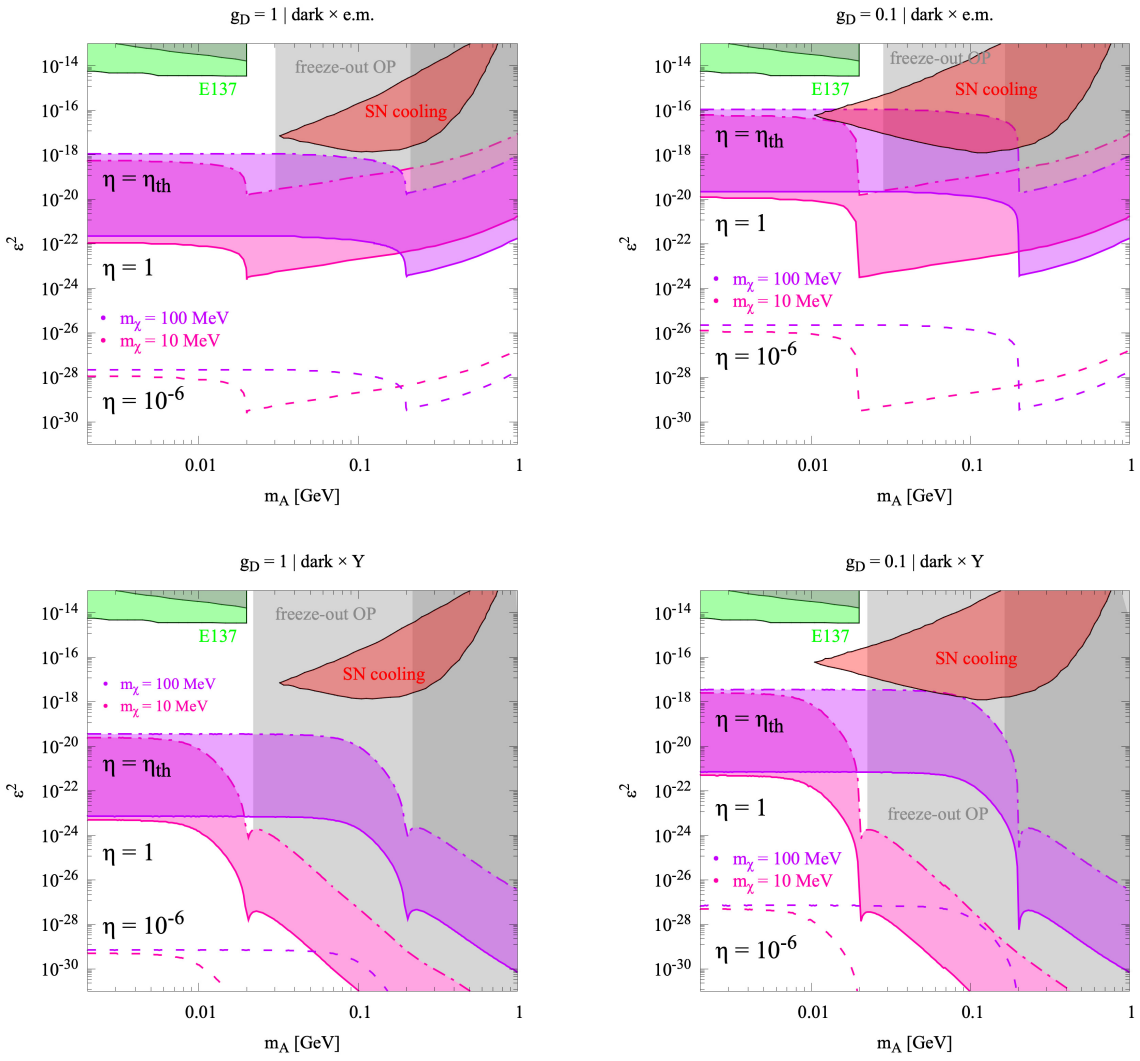

Figure 6. Freeze-in predictions for $g_D = 1$, $g_D = 0.1$ and DM mass $m_\chi = 10\,\text{MeV}$ (magenta lines), $m_\chi = 100\,\text{MeV}$ (purple lines); the top panels show the predictions for a dark × electromagnetic model, while the bottom panels those for a dark × Y/L model, both including an η parameter to account for additional, non-freeze-in DM production. Specifically, $\eta = 1$ (solid lines) refers to a fully thermal model where DM is produced by a freeze-in mechanism; $\eta = 10^{-6}$ (dashed lines) represent a case where thermal mechanisms are responsible only for a small fraction of the total relic density, hence requiring weaker interaction to fulfill the cosmological requirement. Finally, the $\eta > 1$ regions (magenta and purple areas for $m_\chi = 10\,\text{MeV}$ and $100\,\text{MeV}$, respectively) illustrate the parameters' configurations for which the relic abundance is overproduced up to η_{th} (dot-dashed lines) when thermal equilibrium is reached. Freeze-out overproduction is instead represented by grey regions (light grey for $m_\chi = 10\,\text{MeV}$ and dark grey for $m_\chi = 100\,\text{MeV}$). Experimental data such as those from SN cooling and beam dump experiments are currently unable to constraint freeze-in DM with $\Omega h^2 = 0.12$, and are even less sensitive to non-fully thermal models.

JCAP03(2023)061

controlled paradigm instead (dark grey regions). As a marginal note, we point out that for the sake of clarity we omitted references to over-produced DM during the freeze-out discussion, to better analyze them in the following subsection.

SN events may produce sufficiently light particles like axions or DPs, in our case possibly emitted through channels $p+p \to p+p+A'$ and $p+n \to p+n+A'$ via both bremsstrahlung and pion emission. The emission of new physics light degrees of freedom generically alters the supernova energy loss rate. The maximum energy loss allowed by observations of SN1987A [27] reads

$$\epsilon = \frac{L}{M} \sim 10^{19}\,\frac{\mathrm{erg}}{\mathrm{g\,s}}, \tag{3.13}$$

where M is the supernova mass and L its luminosity. This yields a lower limit to ϵ; however, for large values of ϵ "trapping" is possible, due to the fact that sufficiently strongly interacting DPs may not be able to escape the supernova before decaying again. Trapping then gives an upper limit on ϵ. If not all of the DM is produced via freeze-in, and thus $\eta < 1$, then SN cooling and beam dumps experiments will play a more negligible role due to smaller interactions between the visible and dark sector.

4 Future searches

In the scenario discussed here, WIMP-like DM candidates and portal DPs lie around the MeV scale. The direct detection of MeV dark matter is challenging, since the recoil energy is well below the threshold sensitivity of most current detectors. In the region $m_{A'} > 1\,\mathrm{MeV}$, probes of the model under consideration include experiments at colliders and beam dumps. In both cases, a resonance is searched for over a smooth background, with a prompt or slightly displaced vertex with respect to the beam interaction point, in case of a collider, while greatly displaced in the case of beam dump experiments.

As far as colliders experiments are concerned, we have already discussed annihilation processes such as $e^+ + e^- \to \gamma + A'$ testable with experiments such as BaBar, but also Bremsstrahlung ($e^- + Z \to e^- + Z + A'$) and pion decays ($\pi^0 \to \gamma A'$) at KLOE. Beam dump experiments, instead, make use of protons or electrons beams with fixed targets to produce dark photons through Bremsstrahlung and meson production. Examples of these are E141, E137 at SLAC and E774 at Fermilab. Improvements in these directions will be taken up by NA62 and NA64$(e)^{++}$ at SPS, CERN [28], FASER and FASER2 at LHC, CERN [29], HPS at Jefferson Laboratory [30], SeaQuest at Fermilab [31], MAGIX detector for Bremsstrahlung productions [32] and MESA accelerator [33]. It is finally worth noticing the effort towards the measurement of millicharged particles below 10 MeV at CERN and SLAC with the proposed LDMX experiment [34–36].

Turning to indirect detection, the annihilation of MeV-scale dark matter might yield a signature at telescopes sensitive to the relevant energy range. Such signatures consist of often unmistakable features in the electromagnetic spectrum. Gamma rays from WIMPs in the 0.5–250 MeV mass range would lie predominantly in the range $\mathcal{O}$(0.1–100 MeV), which includes the $\pi^0 \to \gamma\gamma$ decay peak centered at roughly 70 MeV. This energy domain was last searched for by EGRET [37] and COMPTEL [38]; future telescopes include proposed experiments such as GAMMA-400 [39], Advanced Compton Telescope (ACT) [40], Advanced Energetic Pair Telescope (AdEPT) [41], PANGU [42], GRAMS [43], MAST [44], AMEGO [45], All-Sky-ASTROGAM [46] and GECCO (Galactic Explorer with a Coded Aperture Mask Compton Telescope) [47, 48], which encapsulates at once the principles of a Compton telescope and of

JCAP03(2023)061

a coded-aperture mask telescope. Performance of the latter in MeV dark matter detection has already been studied closely and we will refer to those studies in what follows.

Future CMB surveys will additionally offer constraining power; thermally produced dark matter can, in principle, annihilate (or decay) into electrons and photons, re-ionizing an amount of the neutral baryonic gas during the Dark Age. Free electrons may enlarge the CMB last scattering surface, allowing for measurable imprints on the temperature and polarization anisotropy spectra of CMB. The "annihilation parameter" $p_{\rm ann} = f_{\rm eff}\langle\sigma v\rangle/m_\chi$ encapsulates all the needed information, taking into account the efficiency of ionization injection through annihilation (or decay) with a redshift-independent parameter $f_{\rm eff}$. Operating and upcoming experiments that will improve *Planck* data are BICEP3/KECK Array [49] and South Pole Telescope-3G [50] in Antarctica, Advanced Atacama Cosmology Telescope Polarimeter (AdvACTPol) [51], Cosmology Large Angular Scale Surveyor (CLASS) [52], Simons Array [53] and Simons Observatory [54].

We conclude by comparing the sensitivity reach of three future experimental avenues. In particular we considered NA64^{++} projections for direct detection experiments, GECCO for indirect detection and the Simons Arrays for CMB precision measurements. Predictions are shown in figure 7 with, respectively, blue, dark green and light green lines, for a representative slice of parameter space with $g_D = 1$, $m_\chi = 10\,\text{MeV}$ in the dark $\times$ electromagnetic theory. NA64^{++} becomes increasingly important in the high A' mass region, where, however, Ωh^2 predictions are already ruled out by *Planck*. GECCO and the Simons Array will play a fundamental role in extending the current parameter space sensitivity down to smaller values of ε^2 (roughly by three orders of magnitudes) in the finely-tuned region approximately around $m_{A'} \sim 2m_\chi$, where DM candidates are currently unconstrained.

5 Conclusions

Previous studies on dark photon portal dark matter models analyzed massless force carriers obtained after symmetry breaking from kinetic mixing operators involving the hypercharge boson [55]. The generalization to massive gauge fields was fully studied in ref. [56], and visually portrayed with a suggestive "Mesa" phase diagram: in it, the authors studied different (and sometimes rather contrived) mechanisms for producing DM while varying the model parameters. The result is a "phase diagram" where the "phases" represent different production mechanisms. Moreover, in the literature, scalar mediator fields (like the Higgs portal) have also been entertained (upon which there are already stringent bounds [57]) as well as fermions like the right handed neutrino in the hypothesis of non-thermal DM production.

Here, we focused on a particular configuration within the mentioned "Mesa" diagram, where the DM is assumed to be in equilibrium, allowing freeze-out to take place. We discussed the presence of DPs in the thermal bath, treating their thermalization independently and deriving constraints on the resulting Boltzmann equations. Moreover, we considered, to our knowledge for the first time, strongly interacting Dark Sectors, which yield novel results for thermal freeze-out.

We considered the most significant experimental constraints, and additionally considered non-standard cosmological setups such as a late-time inflationary period to broaden the relevant region of parameter space under consideration. We also investigated freeze-in production, again taking into account the presence of DPs and their possibly strong interactions with DM. Again to entertain a broader range of possible parameters, we assumed that only part of the DM be produced by freeze-in.

JCAP03(2023)061

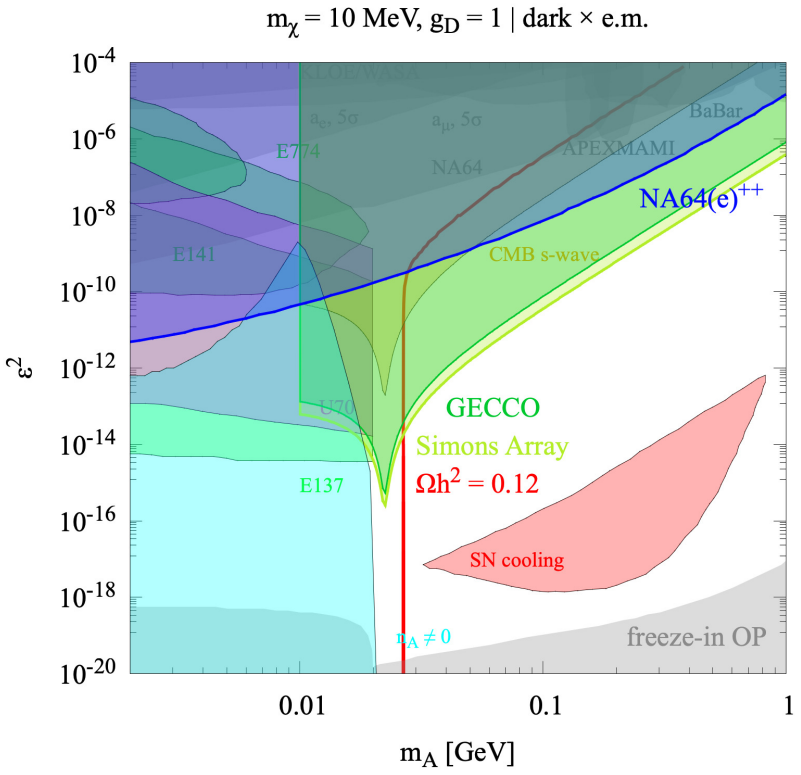

Figure 7. In a specific $m_\chi = 10\,\text{MeV}$ freeze-out scenario, we show predictions for the sensitivity of the future direct detection experiment NA64^{++} [28], and for indirect searches for DM with the GECCO telescopes [47, 48] and with precision CMB measurements by the Simons Array [53].

Our main conclusions are that the general setup accommodates the observed relic abundance for highly constrained configurations in parameter space: $m_\chi \sim m_{A'}$ in the $\varepsilon^2(m_{A'})$-plane, for dark × electromagnetic, $\varepsilon^2 \lesssim 10^{-14}$ when $(m_{A'} = 26.6\,\text{MeV}, g_D = 1)$, $(m_{A'} = 22.5\,\text{MeV}, g_D = 10^{-1})$ whilst for dark × Y, $\varepsilon^2 \lesssim 10^{-18}$ when $(m_{A'} = 21.6\,\text{MeV}, g_D = 1)$ and $\varepsilon^2 \lesssim 10^{-17}$ when $(m_{A'} = 22.1\,\text{MeV}, g_D = 10^{-1})$. In the case of freeze-out scenario, two regions emerged: the first corresponds to when $m_{A'} < m_\chi$ and DM production is driven by the interaction $\chi\chi \to A'A'$ and manifestly appears to be independent by mixing parameter ε^2; a second one when $m_{A'} > m_\chi$ and the process $\chi\chi \to ff$ dominates. In particular, when $m_{A'} < m_\chi$ for both cases $m_\chi = 10\,\text{MeV}$ and $m_\chi = 100\,\text{MeV}$, we get a sharp prediction for g_D independent of ε^2. We then turned to considering a heavier candidate $m_\chi = 100\,\text{MeV}$ that allowed us also to introduce a new phenomenological parameter, a "dilution parameter" Δ stemming from a hypothetical late inflationary period, possibly driven by a classical scalar field. For this new class of models we derived the same predictions relating $\varepsilon^2(m_{A'})$ and $g_D(m_{A'})$ and highlighted some interesting differences between these models and those with a lighter DM mass; in particular we found a non trivial intersection between our density parameter contour plot and the $n_{A'} \neq 0$ region which excluded DM candidates around the singular behaviour of Ωh^2. In summary, in the case of freeze-out production we find that an important subspace region corresponds to a "strong" dark force — $g_D \gtrsim 1$, where experimental bounds are generally weak, while small regions of interest are still present for small values of g_D, especially considering late time inflation.

JCAP03(2023)061

In the freeze-in case, we considered both the presence and absence of DPs in connection with DM production and found out that equilibrium is almost immediately reached if the DPs are present. Assuming $n_{A'} = 0$ we solved simplified Boltzmann equations obtaining again contour plots in the $\varepsilon^2(m_{A'})$-plane, noting that the DM is mainly produced by electron-positron pairs with light quarks contributing at most $\sim 1\%$ to Ωh^2. We found that SN cooling bounds are the closest to constrain model predictions, but are still unable to reach the preferred region of parameter space due to the extremely small kinetic mixing parameter.

Finally we reviewed direct, indirect and CMB measurements future experiments in a particular (and representative) slide of parameters space. We saw that indirect and CMB measures will play an important role in constraining our models in the $m_\chi \sim m_{A'}$ region, where the dependency on ε^2 disappears. Future MeV gamma-ray telescopes and precision CMB surveys will significantly extend the discovery potential of the MeV DM/DP models we considered here.

Acknowledgments

S.P. is partly supported by the U.S. Department of Energy grant number de-sc0010107. N.F. acknowledges support from: *Department of Excellence* grant awarded by the Italian Ministry of Education, University and Research (MIUR); research grant *The Dark Universe: A Synergic Multimessenger Approach*, Grant No. 2017X7X85K funded by the Italian Ministry of Education, University and Research (MIUR); research grant *TAsP (Theoretical Astroparticle Physics)* funded by Istituto Nazionale di Fisica Nucleare (INFN). F.C. thanks Maíra Dutra for fruitful conversations and her help during the initial part of the work.

A Thermal averaged cross section

Fundamental ingredient in Boltzmann equations (3.1) are thermal averaged cross sections whose general expression is

$$\langle \sigma v_{\rm M} \rangle = \frac{\int d^3p_1\, d^3p_2\, f(p_1) f(p_2) \sigma v_{\rm M}}{\int d^3p_1\, d^3p_2\, f(p_1) f(p_2)} \tag{A.1}$$

If we ignore quantum corrections to phase space distributions i.e. assume Maxwell-Boltzmann distributions $f(p) = \exp(-E/T)$, we may manipulate (A.1) up to the point where we're forced to specify $\sigma v_{\rm M}$.

- For a $\mathrm{a}_{(p_1,E_1)} + \mathrm{a}_{(p_2,E_2)} \to \mathrm{b}_{(k_1,\omega_1)} + \mathrm{b}_{(k_2,\omega_2)}$ process (e.g. $\chi\chi \to ff$) we perform a change of variables ϕ such that

$$\phi : \begin{cases} E_+ = E_1 + E_2 \\ E_- = E_1 - E_2 \\ s = 2m_1^2 + 2E_1E_2 - 2p_1p_2\cos\vartheta \end{cases}$$

  transforming volume element and boundaries as

$$d^3p_1\, d^3p_2 = 8\pi^2 E_1 p_1 E_2 p_2\, dE_1\, dE_2\, d\cos\vartheta \overset{\phi}{=} 2\pi^2 E_1 E_2\, dE_+\, dE_-\, ds$$

$$\begin{cases} E_1 \geq m_1^2 \\ E_2 \geq m_1^2 \\ |\cos\vartheta| \leq 1 \end{cases} \overset{\phi}{\to} \begin{cases} s \geq 4m_1^2 \\ E_+ \geq \sqrt{s} \\ |E_-| \leq \sqrt{1 - \frac{4m_1^2}{s}}\sqrt{E_+^2 - s} \end{cases}$$

obtaining

$$\langle \sigma v_{\mathrm{M}_{\mathrm{a+a\to b+b}}} \rangle = \frac{2\pi^2 T g_{\mathrm{a}}^2}{(2\pi)^6 (n_{\mathrm{a}}^{\mathrm{eq}})^2} \int_{4m_1^2}^{\infty} ds\, \sqrt{s} K_1(\sqrt{s}/T) \left(s - 4m_1^2\right) \sigma_{\mathrm{aa\to bb}} \tag{A.2}$$

- For a $\mathrm{a}_{(p_1,E_1)}+\mathrm{b}_{(k_1,\omega_1)} \to \mathrm{a}_{(p_2,E_2)}+\mathrm{b}_{(k_2,\omega_2)}$ process (e.g. $\chi A' \to \chi A'$), change of variables ϕ is in the form

$$\phi : \begin{cases} E_+ = E_1 + \omega_1 \\ E_- = E_1 - \omega_1 \\ s = m_1^2 + m_2^2 + 2E_1\omega_1 - 2p_1 k_1 \cos\vartheta \end{cases}$$

hence

$$d^3p_1\, d^3k_1 = 8\pi^2 E_1 p_1 \omega_1 k_1\, dE_1\, d\omega_1\, d\cos\vartheta \overset{\phi}{=} 2\pi^2 E_1 \omega_1\, dE_+\, dE_-\, ds$$

$$\begin{cases} E_1 \geq m_1^2 \\ \omega_1 \geq m_2^2 \\ |\cos\vartheta| \leq 1 \end{cases} \overset{\phi}{\to} \begin{cases} s \geq (m_1+m_2)^2 \\ E_+ \geq \sqrt{s} \\ |E_- - E_+| \leq \sqrt{E_+^2 - s}\sqrt{1 - \frac{2(m_1^2+m_2^2)}{s} - \frac{2m_1^2 m_2^2 - m_1^4 - m_2^4}{s^2}} \end{cases}$$

and

$$\begin{aligned} \langle \sigma v_{\mathrm{M}_{\mathrm{a+b\to a+b}}} \rangle = {} & \frac{2\pi^2 T g_{\mathrm{a}} g_{\mathrm{b}}}{(2\pi)^6 (n_{\mathrm{a}}^{\mathrm{eq}})(n_{\mathrm{b}}^{\mathrm{eq}})} \int_{(m_1+m_2)^2}^{\infty} ds\, \sqrt{s} K_1(\sqrt{s}/T) \\ & \times \left(s - 2(m_1^2+m_2^2) - \frac{2m_1^2 m_2^2 - m_1^4 - m_2^4}{s} \right) \sigma_{\mathrm{ab\to ab}}\,. \end{aligned} \tag{A.3}$$

We now have to turn to σ, recalling that

$$\frac{d\sigma_{\mathrm{aa\to bb}}}{d\cos\vartheta} = \frac{1}{32\pi s} \frac{\sqrt{1-\frac{4m_2^2}{s}}}{\sqrt{1-\frac{4m_1^2}{s}}} |\overline{\mathcal{M}_{\mathrm{aa\to bb}}}|^2$$

$$\frac{d\sigma_{\mathrm{ab\to ab}}}{d\cos\vartheta} = \frac{1}{32\pi s} |\overline{\mathcal{M}_{\mathrm{ab\to ab}}}|^2$$

where we assume azimuthal symmetry and integrate over $\cos\vartheta \in [-1,1]$ for distinguishable final states, while over $\cos\vartheta \in [0,1]$ for indistinguishable final states.

A.1 *s*-channel (electromagnetic)

The amplitude in this case is just

$$\mathcal{M} = \mathcal{M}_{\chi\chi\to A'\to ff}$$

as we represented in figure 8. Hence

$$\begin{aligned} |\overline{\mathcal{M}}|^2 = {} & 4\left(\varepsilon e q_f g_D\right)^2 \left[1 + \frac{4m_\chi^2}{s} + \frac{4m_f^2}{s} + \cos^2\vartheta \left(1 - \frac{4m_\chi^2}{s}\right)\left(1 - \frac{4m_f^2}{s}\right) \right] \\ & \times \frac{s^2}{\left(s^2 - m_{A'}^2\right)^2 + m_{A'}^2 \Gamma_{A'}^2} \end{aligned}$$

$$\sigma_{\chi\chi\to ff} = \frac{(e q_f g_D \varepsilon)^2}{12\pi} \left(1 + \frac{2m_f^2}{s}\right)\left(1 + \frac{2m_\chi^2}{s}\right) \frac{\sqrt{1-\frac{4m_f^2}{s}}}{\sqrt{1-\frac{4m_\chi^2}{s}}} \frac{s}{(s-m_{A'}^2)^2 + m_{A'}^2\Gamma_{A'}^2}\,.$$

JCAP03(2023)061

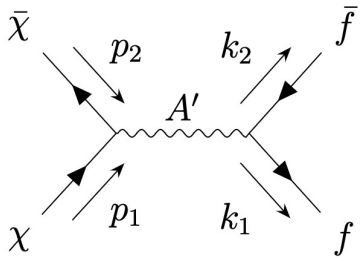

Figure 8. DM annihilating through s-channel into a pair of fermions via the kinetic mixed electromagnetic theory.

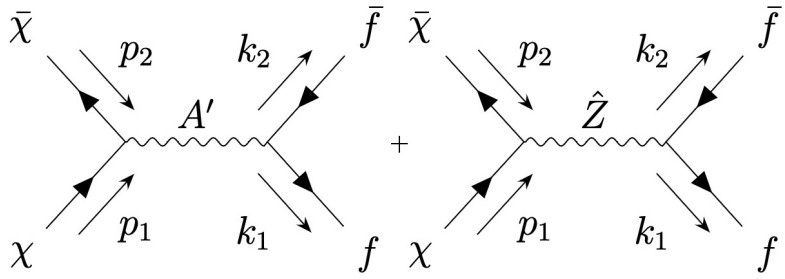

Figure 9. DM annihilating through s-channel into a pair of fermions via the kinetic mixed Y/L theory. This situation requires the sum of two amplitudes coming from the presence of couplings between dark sector and the modified $\hat{Z}$ boson.

A.2 s-channel (Y/L)

Referring to figure 9 we now got to consider the interference between the two process:

$$\mathcal{M} = \mathcal{M}_{\chi\chi\to A'\to ff} + \mathcal{M}_{\chi\chi\to \hat{Z}\to ff}$$

hence

$$\begin{aligned}
|\overline{\mathcal{M}}|^2 = & \frac{\left(s^2 + 4s(m_f^2 + m_\chi^2)\right) + \cos^2\vartheta(s - 4m_f^2)(s - 4m_\chi^2)}{[(s - m_{A'}^2)^2 + m_{A'}^2\Gamma_{A'}^2][(s - m_{\hat{Z}}^2)^2 + m_{\hat{Z}}^2\Gamma_{\hat{Z}}^2]} \\
& \times [(g_f^{A'})^2(g_\chi^{A'})^2((s - m_{\hat{Z}}^2)^2 + m_{\hat{Z}}^2\Gamma_{\hat{Z}}^2) - 2g_f^{A'}g_\chi^{A'}g_f^{\hat{Z}}g_\chi^{\hat{Z}} \\
& \times ((s - m_{A'}^2)(s - m_{\hat{Z}}^2) - m_{A'}m_{\hat{Z}}\Gamma_{A'}\Gamma_{\hat{Z}}) + (g_f^{\hat{Z}})^2(g_\chi^{\hat{Z}})^2((s - m_{A'}^2)^2 + m_{A'}^2\Gamma_{A'}^2)] \\
\sigma_{\chi\chi\to ff} = & \frac{s}{6[(s - m_{A'}^2)^2 + m_{A'}^2\Gamma_{A'}^2][(s - m_{\hat{Z}}^2)^2 + m_{\hat{Z}}^2\Gamma_{\hat{Z}}^2]} \frac{\sqrt{1 - \frac{4m_f^2}{s}}}{\sqrt{1 - \frac{4m_\chi^2}{s}}} \\
& \times \left(1 + \frac{2m_f^2}{s}\right)\left(1 + \frac{2m_\chi^2}{s}\right)\{(g_f^{A'})^2(g_\chi^{A'})^2[(s - m_{\hat{Z}}^2)^2 + m_{\hat{Z}}^2\Gamma_{\hat{Z}}^2] + 2g_f^{A'}g_\chi^{A'}g_f^{\hat{Z}}g_\chi^{\hat{Z}} \\
& \times [(s - m_{A'}^2)(s - m_{\hat{Z}}^2) - m_{A'}m_{\hat{Z}}\Gamma_{A'}\Gamma_{\hat{Z}}] + (g_f^{\hat{Z}})^2(g_\chi^{\hat{Z}})^2[(s - m_{A'}^2)^2 + m_{A'}^2\Gamma_{A'}^2]\}\,.
\end{aligned}$$

JCAP03(2023)061

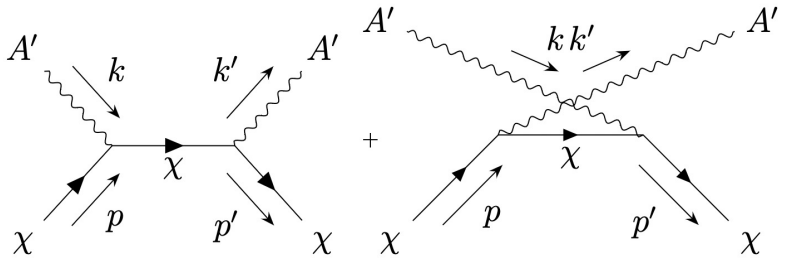

Figure 10. Scattering between DM and DP must take into account the indistinguishability of the initial and final DPs.

A.3 DM-DP scattering

Consider now the DM-DP scattering process in figure 10, the squared amplitude reads

$$|\overline{\mathcal{M}}|^2 = \frac{g_D^2}{6}\left(-\eta_{\nu\beta}+\frac{k_\nu k_\beta}{m_{A'}^2}\right)\left(-\eta_{\mu\alpha}+\frac{k'_\mu k'_\alpha}{m_{A'}^2}\right)\left[\frac{\mathbf{I}}{\left(m_{A'}^2+2pk\right)^2}\right.$$
$$\left.+\frac{\mathbf{II}}{\left(m_{A'}^2+2pk\right)\left(m_{A'}^2-2pk'\right)}+\frac{\mathbf{III}}{\left(m_{A'}^2-2pk'\right)\left(m_{A'}^2+2pk\right)}+\frac{\mathbf{IV}}{\left(m_{A'}^2-2pk'\right)^2}\right] \tag{A.4}$$

where

$$\begin{aligned}
\mathbf{I} &\equiv \mathrm{tr}\left[(\not{p}'+m_\chi)(\gamma^\alpha \not{k}\gamma^\beta+2\gamma^\alpha p^\beta)(\not{p}+m_\chi)(\gamma^\nu \not{k}\gamma^\mu+2\gamma^\mu p^\nu)\right]\\
\mathbf{II} &\equiv \mathrm{tr}\left[(\not{p}'+m_\chi)(\gamma^\alpha \not{k}\gamma^\beta+2\gamma^\alpha p^\beta)(\not{p}+m_\chi)(-\gamma^\mu \not{k}'\gamma^\nu+2\gamma^\nu p^\mu)\right]\\
\mathbf{III} &\equiv \mathrm{tr}\left[(\not{p}'+m_\chi)(-\gamma^\beta \not{k}'\gamma^\alpha+2\gamma^\beta p^\alpha)(\not{p}+m_\chi)(\gamma^\nu \not{k}\gamma^\mu+2\gamma^\mu p^\nu)\right]\\
\mathbf{IV} &\equiv \mathrm{tr}\left[(\not{p}'+m_\chi)(-\gamma^\beta \not{k}'\gamma^\alpha+2\gamma^\beta p^\alpha)(\not{p}+m_\chi)(-\gamma^\mu \not{k}'\gamma^\nu+2\gamma^\nu p^\mu)\right].
\end{aligned}$$

Using *FeynCalc* [58] for contractions we get

$$\begin{aligned}
\sigma_{\chi A'\to\chi A'} = \frac{g_D^4}{24\pi s(s-m_\chi^2)^2}\Bigg\{&\frac{2s(s-m_\chi^2)(s^2-3m_\chi^4-m_\chi^2(6s-4m_{A'}^2)+8m_{A'}^4-4m_{A'}^2 s)}{m_\chi^4-2m_\chi^2(m_{A'}^2+s)+(s-m_{A'}^2)^2}\\
&\times\log\left[\frac{s(s-m_\chi^2-2m_{A'}^2)}{sm_\chi^2-(m_\chi-m_{A'})^2}\right]\\
&+\frac{s^4(m_\chi^2+m_{A'}^2)(13m_\chi^2+m_{A'}^2)+m_\chi^2(m_\chi^2-m_{A'}^2)^4(m_\chi^2+2m_{A'}^2)+m_\chi^2 s^5}{s(m_\chi^2+2m_{A'}^2-s)(m_\chi^4-m_\chi^2(s+2m_{A'}^2)+m_{A'}^4)}\\
&-\frac{s^3(30m_\chi^6+24m_\chi^4m_{A'}^2+13m_\chi^2m_{A'}^4+4m_{A'}^6)-s(m_\chi^2-m_{A'}^2)^2(3m_\chi^6-2m_\chi^4m_{A'}^2}{}\\
&-\underline{8m_\chi^2m_{A'}^4-2m_{A'}^6)+s^2(18m_\chi^8+4m_\chi^6m_{A'}^2-19m_\chi^4m_{A'}^4-8m_\chi^2m_{A'}^6+11m_{A'}^8)}\Bigg\}.
\end{aligned}$$

JCAP03(2023)061

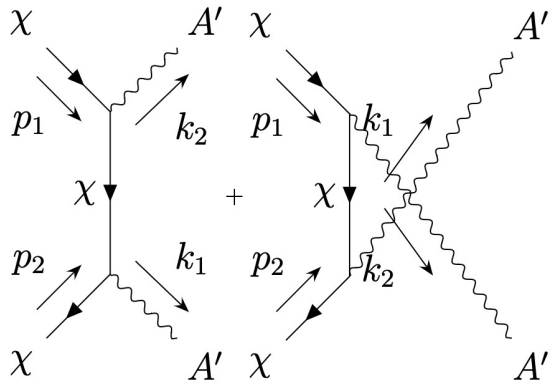

Figure 11. DM annihilation in the t and u channels can be immediately derived by means of crossing symmetry from the results obtained before.

A.4 t and u channels

For the processes in figure 11, we obtained immediately, by means of crossing symmetry on (A.4):

$$p \to p_1, \quad p' \to -p_2 \quad k \to -k_1 \quad k' \to k_2 \tag{A.5}$$

being careful of substituting

- $t = m_\chi^2 + m_{A'}^2 - \frac{s}{2}\left(1 - \sqrt{1-\frac{4m_\chi^2}{s}}\sqrt{1-\frac{4m_{A'}^2}{s}}\cos\vartheta\right)$ in place of $t = (k-k')^2 = 2(\cos\vartheta - 1)(\omega^2 - m_{A'}^2)$,
- adjusting for the degrees of freedom we're averaging with,
- multiplying for (-1) to fix the sign altered by the transformation (A.5).

We get:

$$\begin{aligned}
\sigma_{\chi\chi\to A'A'} = \frac{g_D^4}{32\pi s(s-4m_\chi^2)^2}\frac{\sqrt{1-\frac{4m_{A'}^2}{s}}}{\sqrt{1-\frac{4m_\chi^2}{s}}}\Bigg\{ & \frac{2(s-m_\chi^2)}{\sqrt{s-4m_\chi^2}\sqrt{s-4m_{A'}^2}} \\
& \times\left[-3m_\chi^4 + m_\chi^2(4m_{A'}^2-6s) + 8m_{A'}^4 - 4m_{A'}^2 s + s^2\right] \\
& \times\log\left[\frac{(s-2m_{A'}^2)^2(s-2m_{A'}^2-\sqrt{s-4m_\chi^2}\sqrt{s-4m_{A'}^2})}{4\left[m_{A'}^4 + m_\chi^2(s-4m_{A'}^2)\right](s-2m_{A'}^2+\sqrt{s-4m_\chi^2}\sqrt{s-4m_{A'}^2})}\right] \\
& -2(s-m_\chi^2)^2(2m_\chi^2+m_{A'}^2)^2\left[\frac{4}{\sqrt{s-4m_\chi^2}\sqrt{s-4m_{A'}^2}(s-2m_{A'}^2)}\right. \\
& \left.-\frac{(s-2m_{A'}^2)}{\sqrt{s-4m_\chi^2}\sqrt{s-4m_{A'}^2}\left[m_{A'}^4+m_\chi^2(s-4m_{A'}^2)\right]} + \frac{1}{\left[m_{A'}^4+m_\chi^2(s-4m_{A'}^2)\right]}\right] \\
& -\frac{1}{2}\sqrt{s-4m_\chi^2}\sqrt{s-4m_{A'}^2}(s-m_\chi^2) - m_\chi^2(2m_{A'}^2+7s) - 2m_{A'}^4 - 6m_{A'}^2 s - s^2\Bigg\}.
\end{aligned}$$

JCAP03(2023)061

B Electromagnetic mixing

Starting from Lagrangian density given in (2.1), rotate into the mass eigenstates:

$$\begin{pmatrix} \tilde{A}'_\mu \\ \tilde{A}_\mu \end{pmatrix} = \begin{pmatrix} \frac{1}{\sqrt{1-\varepsilon^2}} & 0 \\ \frac{\varepsilon}{\sqrt{1-\varepsilon^2}} & 1 \end{pmatrix} \begin{pmatrix} \mathrm{c} & -\mathrm{s} \\ \mathrm{s} & \mathrm{c} \end{pmatrix} \begin{pmatrix} A'_\mu \\ A_\mu \end{pmatrix} \tag{B.1}$$

where $\mathrm{c},\, \mathrm{s} = \cos\vartheta,\, \sin\vartheta$, we diagonalize the kinetic terms, while by setting $c \to 1$, $s \to 0$ we obtain the following currents:

$$\mathcal{L}_{\text{int}} \overset{\varepsilon^2 \ll 1}{\sim} g_D J'_\mu A'^\mu + e J_\mu \left(\varepsilon A'^\mu + A^\mu\right) \tag{B.2}$$

Here A_μ is the classical SM photon, while A'_μ is the brand new DP, whose mass acquiring mechanism won't be addressed here, but may be obtained gauge-invariantly through a new Higgs sector or a Stueckelberg Lagrangian [59].

We may notice that this model comprises of a SM photon and a DP coupling directly to DM through g_D and to SM charged fermions through εe: in other words, DM is totally blind to known interactions, except for gravity, and it can only be seen by means of the new force carrier DP. Notice we used the fact that $|\varepsilon|^2 \ll 1$ which is known to be true for instance from the "milli-charged" DM phenomenology, which is by the way obtainable within the same construction depicted above setting $\mathrm{s} \to -\varepsilon$, $\mathrm{c} \to \sqrt{1-\varepsilon^2}$:

$$\begin{aligned} \mathcal{L}_{\text{int}} &= \left(\frac{g_D}{\sqrt{1-\varepsilon^2}}\varepsilon J'_\mu + \frac{e}{\sqrt{1-\varepsilon^2}}\varepsilon J_\mu\right) A^\mu + g_D J'_\mu A'^\mu \\ &\overset{|\varepsilon|^2 \ll 1}{\sim} (g_D \varepsilon J'_\mu + e\varepsilon J_\mu) A^\mu + g_D J'_\mu A'^\mu \,. \end{aligned} \tag{B.3}$$

Notice how in this case, we're dealing with a electrically charged DM which directly interacts with the SM whilst the DP plays no role (at tree level, at least) and it gets secluded to the sole DS.

C Hypercharge mixing

Here we start from Lagrangian (2.2), first by recalling all the present covariant derivatives

$$\begin{aligned} \mathcal{D}_\mu \Phi &= \left(\partial_\mu - i\frac{1}{2} g_2 W^3_\mu \sigma^3 - i\frac{1}{2} g_1 B_\mu\right) \Phi \\ \mathcal{D}_\mu L &= \left(\partial_\mu - i\frac{1}{2} g_2 W^3_\mu \sigma^3 - i\frac{1}{2} g_1 B_\mu\right) L \\ \mathcal{D}_\mu \ell_{\mathrm{R}} &= \left(\partial_\mu + i g_1 B_\mu\right) \ell_{\mathrm{R}} \\ \mathcal{D}_\mu Q &= \left(\partial_\mu - i\frac{1}{2} g_2 \sigma^3 W^3_\mu - i\frac{1}{6} g_1 B_\mu\right) Q \\ \mathcal{D}_\mu u_{\mathrm{R}} &= \left(\partial_\mu - i\frac{2}{3} g_1 B_\mu\right) u_{\mathrm{R}} \\ \mathcal{D}_\mu d_{\mathrm{R}} &= \left(\partial_\mu + i\frac{1}{3} g_1 B_\mu\right) d_{\mathrm{R}} \\ \mathcal{D}_\mu \chi &= \left(\partial_\mu + i g_D a'_\mu\right) \chi \end{aligned}$$

excluding charged boson within $\mathrm{SU}(2)_{\mathrm{L}}$ for simplicity.

JCAP03(2023)061

We perform the first transformation to diagonalize the kinetic sector:

$$\begin{pmatrix} B_\mu \\ W^3_\mu \\ a'_\mu \end{pmatrix} = G_{\rm Y}(\varepsilon) \begin{pmatrix} \tilde{B}_\mu \\ \tilde{W^3}_\mu \\ \tilde{a'}_\mu \end{pmatrix}$$

with

$$G_{\rm Y}(\varepsilon) = \begin{pmatrix} 1 & 0 & -\frac{\varepsilon}{\sqrt{1-\varepsilon^2}} \\ 0 & 1 & 0 \\ 0 & 0 & \frac{1}{\sqrt{1-\varepsilon^2}} \end{pmatrix} .$$

Let now the Higgs acquire a VEV (ignoring ϕ^+, ϕ^- and ϕ^0):

$$\Phi \to \frac{1}{\sqrt{2}} \begin{pmatrix} v+H \\ 0 \end{pmatrix}$$

and substitute the former transformation in the mass term of (2.2):

$$\mathcal{L}_{\rm mass} = \frac{1}{2} \left(\tilde{B}_\mu \ \tilde{W^3}_\mu \ \tilde{a}'_\mu \right) \frac{v^2}{4} \begin{pmatrix} g_1^2 & -g_1 g_2 & -g_1^2 \varepsilon \\ -g_1 g_2 & g_2^2 & g_1 g_2 \varepsilon \\ -g_1^2 \varepsilon & g_1 g_2 \varepsilon & g_1^2 \varepsilon^2 + \frac{4 m^2_{a'} (1+\varepsilon^2)}{v^2} \end{pmatrix} \begin{pmatrix} \tilde{B}_\mu \\ \tilde{W^3}_\mu \\ \tilde{a}'_\mu \end{pmatrix} .$$

Finally define the mass eigenstates through orthogonal transformation P such that:

$$\begin{pmatrix} \tilde{B}_\mu \\ \tilde{W^3}_\mu \\ \tilde{a}'_\mu \end{pmatrix} = {\rm P}^{-1} \begin{pmatrix} A_\mu \\ \hat{Z}_\mu \\ A'_\mu \end{pmatrix}$$

where we defined P to be:

$${\rm P}(\xi, \vartheta_{\rm W}) = R_1(\xi) R_2(\vartheta_{\rm W}) = \begin{pmatrix} 1 & 0 & 0 \\ 0 & \cos\xi & \sin\xi \\ 0 & -\sin\xi & \cos\xi \end{pmatrix} \begin{pmatrix} \cos\vartheta_{\rm W} & \sin\vartheta_{\rm W} & 0 \\ -\sin\vartheta_{\rm W} & \cos\vartheta_{\rm W} & 0 \\ 0 & 0 & 1 \end{pmatrix}$$

where $\xi = (1/2) \arctan\left(\frac{2\,\varepsilon\,\sin\vartheta_{\rm W}}{1-\delta}\right)$, $\delta = m^2_{a'}/m^2_Z$, $m_Z \simeq 91.2\,{\rm GeV}$ and $\cos\vartheta_{\rm W} \simeq 0.88$. Notice that we distinguished $\hat{Z}$ from Z due to a $\mathcal{O}(\varepsilon^2)$ difference between their masses, discrepancy which is well known in the literature to be a signature of kinetic mixing effects. From these transformations we can read out the eigenvalues from the diagonal mass matrix. Define $\Gamma \equiv 1/(1-\delta)$, $\beth \equiv 1/2(\delta-1)^2$:

$$\begin{aligned} m^2_A &= 0 \\ m^2_{A'} &\sim m_{a'} \{1 + \varepsilon^2 [1 - s^2_{\rm W}(1 + \delta + 3\delta^2)]\} \\ m^2_{\hat{Z}} &\sim m^2_Z (1 + s^2_{\rm W} \varepsilon^2 \Gamma) \end{aligned}$$

JCAP03(2023)061

and applying $G_{\rm Y}(\varepsilon)\mathrm{P}(\xi,\vartheta_{\rm W})^{-1}$ to the currents we find the interacting part of our Lagrangian

$$\begin{aligned}\mathcal{L} = &-\frac{1}{4}F_{\mu\nu}F^{\mu\nu} - \frac{1}{4}\hat{Z}_{\mu\nu}\hat{Z}^{\mu\nu} - \frac{1}{4}F'_{\mu\nu}F'^{\mu\nu} + \frac{1}{2}m^2_{\hat{Z}}\hat{Z}_\mu\hat{Z}^\mu + \frac{1}{2}m^2_{A'}A'_\mu A'^\mu \\ &+ i\bar{L}(g_L^A \not{A} + g_L^{A'}\not{A}' + g_L^{\hat{Z}}\not{\hat{Z}})L + i\bar{\ell}_{\rm R}(g_{\ell_{\rm R}}^A\not{A} + g_{\ell_{\rm R}}^{A'}\not{A}' + g_{\ell_{\rm R}}^{\hat{Z}}\not{\hat{Z}})\ell_{\rm R} \\ &+ \bar{Q}(g_L^A\not{A} + g_Q^{A'}\not{A}' + g_Q^{\hat{Z}}\not{\hat{Z}})Q + \bar{u}_{\rm R}(g_{\ell_{\rm R}}^A\not{A} + g_{u_{\rm R}}^{A'}\not{A}' + g_{u_{\rm R}}^{\hat{Z}}\not{\hat{Z}})u_{\rm R} \\ &+ \bar{d}_{\rm R}(g_{\ell_{\rm R}}^A\not{A} + g_{d_{\rm R}}^{A'}\not{A}' + g_{d_{\rm R}}^{\hat{Z}}\not{\hat{Z}})d_{\rm R} + g_{H\hat{Z}\hat{Z}}H\hat{Z}_\mu\hat{Z}^\mu + g_{HH\hat{Z}\hat{Z}}HH\hat{Z}_\mu\hat{Z}^\mu \\ &+ g_{HA'A'}HA'_\mu A'^\mu + g_{HHA'A'}HHA'_\mu A'^\mu + g_{H\hat{Z}A'}H\hat{Z}_\mu A'^\mu + g_{HH\hat{Z}A'}HH\hat{Z}_\mu A'^\mu\end{aligned} \tag{C.1}$$

with couplings,

$$\begin{aligned}
g_{\nu_L}^{A'} &= -\frac{e\varepsilon}{2c_{\rm W}}(1-\Gamma) \\
g_{\ell_L}^{A'} &= -\frac{e\varepsilon}{2c_{\rm W}}(1-\Gamma+2\Gamma c_{\rm W}^2) \\
g_{\ell_R}^{A'} &= -\frac{e\varepsilon}{c_{\rm W}}(1-s_{\rm W}^2\Gamma) \\
g_{u_L}^{A'} &= \frac{e\varepsilon}{2c_{\rm W}}\left[\frac{1}{3}+\Gamma\left(c_{\rm W}^2-\frac{s_{\rm W}^2}{3}\right)\right] \\
g_{d_L}^{A'} &= \frac{e\varepsilon}{2c_{\rm W}}(s_{\rm W}^2\Gamma-1) \\
g_{u_R}^{A'} &= -\frac{2}{3}\frac{e\varepsilon}{c_{\rm W}}(s_{\rm W}^2\Gamma-1) \\
g_{d_R}^{A'} &= \frac{1}{3}\frac{e\varepsilon}{c_{\rm W}}(s_{\rm W}^2\Gamma-1) \\
g_{\chi}^{A'} &= g_D\left[1+\varepsilon^2\left(\frac{1}{2}-s_{\rm W}^2\text{ℶ}\right)\right] \\
g_{\nu_L}^{\hat{Z}} &= -\frac{e}{2c_{\rm W}s_{\rm W}}+\frac{e\varepsilon^2\tan\vartheta_{\rm W}}{2}(\text{ℶ}-\Gamma) \\
g_{\ell_L}^{\hat{Z}} &= -\frac{e}{2c_{\rm W}s_{\rm W}}(s_{\rm W}^2-c_{\rm W}^2)+\frac{e\varepsilon^2}{2}[\tan\vartheta_{\rm W}(\text{ℶ}-\Gamma)-2s_{\rm W}c_{\rm W}] \\
g_{\ell_R}^{\hat{Z}} &= -e\tan\vartheta_{\rm W}+\frac{e\varepsilon^2}{c_{\rm W}}[s_{\rm W}(\text{ℶ}-\Gamma)-c_{\rm W}^2\text{ℶ}] \\
g_{u_L}^{\hat{Z}} &= \frac{e}{2}\left(\frac{1}{3}\tan\vartheta_{\rm W}-\cot\vartheta_{\rm W}\right)-\frac{e\varepsilon^2}{2}\left[\frac{1}{3}\tan\vartheta_{\rm W}(\text{ℶ}-\Gamma)-\frac{4}{3}s_{\rm W}c_{\rm W}\text{ℶ}\right] \\
g_{d_L}^{\hat{Z}} &= \frac{e}{2}\left(\frac{1}{3}\tan\vartheta_{\rm W}+\cot\vartheta_{\rm W}\right)-\frac{e\varepsilon^2}{2}\left[\frac{2}{3}c_{\rm W}s_{\rm W}\text{ℶ}+\frac{1}{3}\tan\vartheta_{\rm W}(\text{ℶ}-\Gamma)\right] \\
g_{u_R}^{\hat{Z}} &= \frac{2}{3}e\tan\vartheta_{\rm W}-\frac{2}{3}e\varepsilon^2[\tan\vartheta_{\rm W}(\text{ℶ}-\Gamma)-s_{\rm W}c_{\rm W}\text{ℶ}] \\
g_{d_R}^{\hat{Z}} &= -\frac{1}{3}e\tan\vartheta_{\rm W}+\frac{1}{3}e\varepsilon^2[\tan\vartheta_{\rm W}(\text{ℶ}-\Gamma)-s_{\rm W}c_{\rm W}\text{ℶ}] \\
g_{\chi}^{\hat{Z}} &= g_D\varepsilon s_{\rm W}\Gamma
\end{aligned}$$

JCAP03(2023)061

$$
\begin{aligned}
g_{HA'A'} &= \frac{e^2\varepsilon^2}{4c_{\rm W}^2}(\Gamma-1)^2 v \\
g_{HHA'A'} &= \frac{e^2\varepsilon^2}{8c_{\rm W}^2}(\Gamma-1)^2 \\
g_{HA'\hat{Z}} &= -\frac{e^2\varepsilon}{2s_{\rm W}c_{\rm W}}(\Gamma-1)v \\
g_{HHA'\hat{Z}} &= -\frac{e^2\varepsilon}{4s_{\rm W}c_{\rm W}}(\Gamma-1) \\
g_{H\hat{Z}\hat{Z}} &= \frac{e^2}{4s_{\rm W}^2c_{\rm W}^2}v + \frac{e^2\varepsilon^2}{2c_{\rm W}^2}(\Gamma-1)v \\
g_{HH\hat{Z}\hat{Z}} &= \frac{e^2}{8c_{\rm W}^2s_{\rm W}^2} + \frac{e^2\varepsilon^2}{4c_{\rm W}^2}(\Gamma-1)\,.
\end{aligned}
$$

D Isospin mixing

The mathematics for this model is almost the same one used in [C]. We just need to substitute $G_{\rm Y}$ with

$$
G_{\rm L}(\varepsilon) = \begin{pmatrix} 1 & 0 & 0 \\ 0 & 1 & -\frac{\varepsilon}{\sqrt{1-\varepsilon^2}} \\ 0 & 0 & \frac{1}{\sqrt{1-\varepsilon^2}} \end{pmatrix} . \tag{D.1}
$$

After diagonalizing the mass matrix and applying $G_{\rm L}(\varepsilon){\rm P}(\xi,\vartheta_{\rm W})^{-1}$ to the currents terms we get the followings eigenvalues and couplings:

$$
\begin{aligned}
m_A^2 &= 0 \\
m_{A'}^2 &\sim m_{a'}^2\left\{1+\varepsilon^2\left[\frac{1}{2\delta}(3+4c_{\rm W}s_{\rm W}-2s_{\rm W}^2)+(1+\delta)(2+2c_{\rm W}s_{\rm W}-s_{\rm W}^2)\right]\right\} \\
m_{\hat{Z}}^2 &\sim m_Z^2[1-\varepsilon^2(2c_{\rm W}s_{\rm W}+s_{\rm W}^2)\Gamma] \\
g_{\nu_L}^{A'} &= \frac{e\varepsilon}{2}\left(\frac{1}{s_{\rm W}}+\frac{\Gamma}{c_{\rm W}}\right) \\
g_{\ell_L}^{A'} &= -\frac{e\varepsilon}{2s_{\rm W}}\left(1-\frac{s_{\rm W}}{c_{\rm W}}(2s_{\rm W}^2-1)\Gamma\right) \\
g_{\ell_R}^{A'} &= e\varepsilon\frac{s_{\rm W}^2}{c_{\rm W}}\Gamma \\
g_{u_L}^{A'} &= \frac{e\varepsilon}{2}\left[\frac{1}{s_{\rm W}}+s_{\rm W}\left(\cot\vartheta_{\rm W}-\frac{1}{3}\tan\vartheta_{\rm W}\right)\Gamma\right] \\
g_{d_L}^{A'} &= -\frac{e\varepsilon}{2}\left[\frac{1}{s_{\rm W}}+\frac{1}{c_{\rm W}}\left(c_{\rm W}^2+\frac{1}{3}s_{\rm W}^2\right)\Gamma\right] \\
g_{u_R}^{A'} &= -\frac{2}{3}e\varepsilon\frac{s_{\rm W}^2}{c_{\rm W}}\Gamma \\
g_{d_R}^{A'} &= \frac{1}{3}e\varepsilon\frac{s_{\rm W}^2}{c_{\rm W}}\Gamma
\end{aligned}
$$

JCAP03(2023)061

$$
\begin{aligned}
g_{\chi}^{A'} &= g_D \left[1 + \varepsilon^2 \left(\frac{1}{2} - s_{\mathrm{W}}^2 \text{⨽}\right)\right] \\
g_{\nu_L}^{\hat{Z}} &= -\frac{e}{2c_{\mathrm{W}}s_{\mathrm{W}}} + \frac{e\varepsilon^2 \tan\vartheta_{\mathrm{W}}}{2}(\tan\vartheta_{\mathrm{W}} \text{⨽} - \Gamma) \\
g_{\ell_L}^{\hat{Z}} &= -\frac{e}{2c_{\mathrm{W}}s_{\mathrm{W}}}(s_{\mathrm{W}}^2 - c_{\mathrm{W}}^2) + \frac{e\varepsilon^2}{2}[\tan\vartheta_{\mathrm{W}}(s_{\mathrm{W}}^2 - c_{\mathrm{W}}^2) \text{⨽} - \Gamma] \\
g_{\ell_R}^{\hat{Z}} &= -e\tan\vartheta_{\mathrm{W}} + e\varepsilon^2 \frac{s_{\mathrm{W}}^3}{c_{\mathrm{W}}} \text{⨽} \\
g_{u_L}^{\hat{Z}} &= \frac{e}{2}\left(\frac{1}{3}\tan\vartheta_{\mathrm{W}} - \cot\vartheta_{\mathrm{W}}\right) + \frac{e\varepsilon^2}{2}\left[\tan\vartheta_{\mathrm{W}}\left(c_{\mathrm{W}}^2 - \frac{1}{3}s_{\mathrm{W}}^2\right) \text{⨽} + \Gamma\right] \\
g_{d_L}^{\hat{Z}} &= \frac{e}{2}\left(\frac{1}{3}\tan\vartheta_{\mathrm{W}} + \cot\vartheta_{\mathrm{W}}\right) - \frac{e\varepsilon^2}{2}\left[\tan\vartheta_{\mathrm{W}}\left(c_{\mathrm{W}}^2 + \frac{1}{3}s_{\mathrm{W}}^2\right) \text{⨽} + \Gamma\right] \\
g_{u_R}^{\hat{Z}} &= \frac{2}{3}e\tan\vartheta_{\mathrm{W}} - \frac{2}{3}e\varepsilon^2\frac{s_{\mathrm{W}}^3}{c_{\mathrm{W}}} \text{⨽} \\
g_{d_R}^{\hat{Z}} &= -\frac{1}{3}e\tan\vartheta_{\mathrm{W}} + \frac{1}{3}e\varepsilon^2\frac{s_{\mathrm{W}}^3}{c_{\mathrm{W}}} \text{⨽} \\
g_{\chi}^{\hat{Z}} &= g_D\varepsilon s_{\mathrm{W}}\Gamma \\
g_{HA'A'} &= \frac{e^2\varepsilon^2}{4c_{\mathrm{W}}^2 s_{\mathrm{W}}^2}(c_{\mathrm{W}} + s_{\mathrm{W}}\Gamma)^2 v \\
g_{HHA'A'} &= \frac{e^2\varepsilon^2}{8c_{\mathrm{W}}^2 s_{\mathrm{W}}^2}(c_{\mathrm{W}} + s_{\mathrm{W}}\Gamma)^2 \\
g_{HA'\hat{Z}} &= -\frac{e^2\varepsilon}{2s_{\mathrm{W}}^2 c_{\mathrm{W}}^2}(c_{\mathrm{W}} + s_{\mathrm{W}}\Gamma)v \\
g_{HHA'\hat{Z}} &= -\frac{e^2\varepsilon}{4s_{\mathrm{W}}^2 c_{\mathrm{W}}^2}(c_{\mathrm{W}} + s_{\mathrm{W}}\Gamma) \\
g_{H\hat{Z}\hat{Z}} &= \frac{e^2}{4s_{\mathrm{W}}^2 c_{\mathrm{W}}^2}v - \frac{e^2\varepsilon^2}{2c_{\mathrm{W}}^2 s_{\mathrm{W}}}(c_{\mathrm{W}}\Gamma - s_{\mathrm{W}} \text{⨽})v \\
g_{HH\hat{Z}\hat{Z}} &= \frac{e^2}{8c_{\mathrm{W}}^2 s_{\mathrm{W}}^2} - \frac{e^2\varepsilon^2}{4c_{\mathrm{W}}^2 s_{\mathrm{W}}}(c_{\mathrm{W}}\Gamma - s_{\mathrm{W}} \text{⨽}) \,.
\end{aligned}
$$

References

[1] Planck collaboration, *Planck 2018 results. Part VI. Cosmological parameters*, *Astron. Astrophys.* **641** (2020) A6 [*Erratum ibid.* **652** (2021) C4] [arXiv:1807.06209] [inSPIRE].

[2] G. 't Hooft, *Renormalizable Lagrangians for Massive Yang-Mills Fields*, *Nucl. Phys. B* **35** (1971) 167 [inSPIRE].

[3] Particle Data collaboration, *Review of Particle Physics*, *Prog. Theor. Exp. Phys.* **2022** (2022) 083C01 [inSPIRE].

[4] V. Springel et al., *Prospects for detecting supersymmetric dark matter in the Galactic halo*, *Nature* **456N7218** (2008) 73 [inSPIRE].

JCAP03(2023)061

[5] G. Arcadi et al., *The waning of the WIMP? A review of models, searches, and constraints*, *Eur. Phys. J. C* **78** (2018) 203 [arXiv:1703.07364] [INSPIRE].

[6] J. Jaeckel and A. Ringwald, *The Low-Energy Frontier of Particle Physics*, *Ann. Rev. Nucl. Part. Sci.* **60** (2010) 405 [arXiv:1002.0329] [INSPIRE].

[7] R. Essig et al., *Working Group Report: New Light Weakly Coupled Particles*, in proceedings of the *Community Summer Study 2013: Snowmass on the Mississippi*, Minneapolis, MN, U.S.A., 29 July–6 August 2013, arXiv:1311.0029 [INSPIRE].

[8] J. Alexander et al., *Dark Sectors 2016 Workshop: Community Report*, arXiv:1608.08632 [INSPIRE].

[9] M. Fabbrichesi, E. Gabrielli and G. Lanfranchi, *The Physics of the Dark Photon*, Springer International Publishing (2021) [DOI:10.1007/978-3-030-62519-1].

[10] T. Asaka, K. Ishiwata and T. Moroi, *Right-handed sneutrino as cold dark matter of the universe*, *Phys. Rev. D* **75** (2007) 065001 [hep-ph/0612211] [INSPIRE].

[11] S. Gopalakrishna, A. de Gouvêa and W. Porod, *Right-handed sneutrinos as nonthermal dark matter*, *JCAP* **05** (2006) 005 [hep-ph/0602027] [INSPIRE].

[12] L.J. Hall, K. Jedamzik, J. March-Russell and S.M. West, *Freeze-In Production of FIMP Dark Matter*, *JHEP* **03** (2010) 080 [arXiv:0911.1120] [INSPIRE].

[13] C. Dvorkin, T. Lin and K. Schutz, *Cosmology of Sub-MeV Dark Matter Freeze-In*, *Phys. Rev. Lett.* **127** (2021) 111301 [arXiv:2011.08186] [INSPIRE].

[14] E.W. Kolb and M.S. Turner, *The Early Universe*, in *Frontiers in Physics* **69**, CRC Press, Boca Raton, FL, U.S.A. (1990) [DOI:10.1201/9780429492860] [INSPIRE].

[15] P. Gondolo and G. Gelmini, *Cosmic abundances of stable particles: Improved analysis*, *Nucl. Phys. B* **360** (1991) 145 [INSPIRE].

[16] S. Andreas, C. Niebuhr and A. Ringwald, *New Limits on Hidden Photons from Past Electron Beam Dumps*, *Phys. Rev. D* **86** (2012) 095019 [arXiv:1209.6083] [INSPIRE].

[17] J. Blümlein and J. Brunner, *New Exclusion Limits for Dark Gauge Forces from Beam-Dump Data*, *Phys. Lett. B* **701** (2011) 155 [arXiv:1104.2747] [INSPIRE].

[18] A1 collaboration, *Search for Light Gauge Bosons of the Dark Sector at the Mainz Microtron*, *Phys. Rev. Lett.* **106** (2011) 251802 [arXiv:1101.4091] [INSPIRE].

[19] S. Abrahamyan et al., *Search for a New Gauge Boson in Electron-Nucleus Fixed-Target Scattering by the APEX Experiment*, *Phys. Rev. Lett.* **107** (2011) 191804 [arXiv:1108.2750] [INSPIRE].

[20] J.D. Bjorken, R. Essig, P. Schuster and N. Toro, *New Fixed-Target Experiments to Search for Dark Gauge Forces*, *Phys. Rev. D* **80** (2009) 075018 [arXiv:0906.0580] [INSPIRE].

[21] BABAR collaboration, *Search for Dimuon Decays of a Light Scalar in Radiative Transitions* $\Upsilon(3S) \to \gamma A^0$, in proceedings of the *2009 Aspen Winter Conference on Astronomy: Thirty Years of Magnetars: New Frontiers*, Aspen, CO, U.S.A., 1–7 February 2009, arXiv:0902.2176 [INSPIRE].

[22] KLOE-2 collaboration, *Search for a vector gauge boson in ϕ meson decays with the KLOE detector*, *Phys. Lett. B* **706** (2012) 251 [arXiv:1110.0411] [INSPIRE].

[23] T.R. Slatyer, *Indirect dark matter signatures in the cosmic dark ages. Part I. Generalizing the bound on s-wave dark matter annihilation from Planck results*, *Phys. Rev. D* **93** (2016) 023527 [arXiv:1506.03811] [INSPIRE].

[24] H.K. Dreiner, J.-F. Fortin, C. Hanhart and L. Ubaldi, *Supernova constraints on MeV dark sectors from e^+e^- annihilations*, *Phys. Rev. D* **89** (2014) 105015 [arXiv:1310.3826] [INSPIRE].

JCAP03(2023)061

[25] H. Davoudiasl, D. Hooper and S.D. McDermott, *Inflatable Dark Matter*, *Phys. Rev. Lett.* **116** (2016) 031303 [arXiv:1507.08660] [INSPIRE].

[26] P.N. Bhattiprolu, G. Elor, R. McGehee and A. Pierce, *Freezing-in hadrophilic dark matter at low reheating temperatures*, *JHEP* **01** (2023) 128 [arXiv:2210.15653] [INSPIRE].

[27] G.G. Raffelt, *Stars as laboratories for fundamental physics: The astrophysics of neutrinos, axions, and other weakly interacting particles*, University of Chicago Press, Chicago, IL, U.S.A. (1996) [ISBN: 978–0–226–70272–8].

[28] S. Gninenko, *Addendum to the NA64 Proposal: Search for the $A' \to$ invisible and $X \to e^+e^-$ decays in 2021*, CERN, Geneva, Switzerland (2018) [CERN-SPSC-2018-004] [SPSC-P-348-ADD-2].

[29] J.L. Feng, I. Galon, F. Kling and S. Trojanowski, *ForwArd Search ExpeRiment at the LHC*, *Phys. Rev. D* **97** (2018) 035001 [arXiv:1708.09389] [INSPIRE].

[30] HEAVY PHOTON SEARCH collaboration, *Search for a dark photon in electroproduced e^+e^- pairs with the Heavy Photon Search experiment at JLab*, *Phys. Rev. D* **98** (2018) 091101 [arXiv:1807.11530] [INSPIRE].

[31] A. Berlin, S. Gori, P. Schuster and N. Toro, *Dark Sectors at the Fermilab SeaQuest Experiment*, *Phys. Rev. D* **98** (2018) 035011 [arXiv:1804.00661] [INSPIRE].

[32] L. Doria, P. Achenbach, M. Christmann, A. Denig, P. Guelker and H. Merkel, *Search for light dark matter with the MESA accelerator*, in proceedings of the *13th Conference on the Intersections of Particle and Nuclear Physics*, Palm Springs, CA, U.S.A., 29 May–3 June 2018, arXiv:1809.07168 [INSPIRE].

[33] L. Doria, P. Achenbach, M. Christmann, A. Denig and H. Merkel, *Dark Matter at the Intensity Frontier: the new MESA electron accelerator facility*, *PoS* **ALPS2019** (2020) 022 [arXiv:1908.07921] [INSPIRE].

[34] T. Åkesson et al., *Light Dark Matter eXperiment (LDMX)*, arXiv:1808.05219 [FERMILAB-PUB-18-324-A] [INSPIRE].

[35] T. Raubenheimer et al., *DASEL: Dark Sector Experiments at LCLS-II*, arXiv:1801.07867 [SLAC-PUB-17225] [INSPIRE].

[36] T. Åkesson et al., *Dark Sector Physics with a Primary Electron Beam Facility at CERN*, CERN, Geneva, Switzerland (2018) [CERN-SPSC-2018-023] [SPSC-EOI-018].

[37] S.D. Hunter et al., *EGRET observations of the diffuse gamma-ray emission from the galactic plane*, *Astrophys. J.* **481** (1997) 205 [INSPIRE].

[38] A.W. Strong, H. Bloemen, R. Diehl, W. Hermsen and V. Schoenfelder, *Comptel skymapping: A New approach using parallel computing*, *Astrophys. Lett. Commun.* **39** (1999) 209 [astro-ph/9811211] [INSPIRE].

[39] A.M. Galper et al., *The GAMMA-400 space observatory: status and perspectives*, arXiv:1412.4239 [INSPIRE].

[40] S.E. Boggs et al., *The Advanced Compton Telescope Mission*, *New Astron. Rev.* **50** (2006) 604 [astro-ph/0608532] [INSPIRE].

[41] S.D. Hunter et al., *A Pair Production Telescope for Medium-Energy Gamma-Ray Polarimetry*, *Astropart. Phys.* **59** (2014) 18 [arXiv:1311.2059] [INSPIRE].

[42] X. Wu et al., *PANGU: A High Resolution Gamma-ray Space Telescope*, in proceedings of the *SPIE Astronomical Telescopes + Instrumentation*, Montréal, Quebec, Canada, 22–27 June 2014, *Proc. SPIE* **9144** (2014) 91440F [arXiv:1407.0710] [INSPIRE].

JCAP03(2023)061

[43] T. Aramaki, P. Hansson Adrian, G. Karagiorgi and H. Odaka, *Dual MeV Gamma-Ray and Dark Matter Observatory — GRAMS Project*, *Astropart. Phys.* **114** (2020) 107 [arXiv:1901.03430] [INSPIRE].

[44] T. Dzhatdoev and E. Podlesnyi, *Massive Argon Space Telescope (MAST): A concept of heavy time projection chamber for γ-ray astronomy in the* 100 *MeV–*1 *TeV energy range*, *Astropart. Phys.* **112** (2019) 1 [arXiv:1902.01491] [INSPIRE].

[45] AMEGO Team collaboration, *AMEGO: Exploring the Extreme Multimessenger Universe*, *Proc. SPIE* **11444** (2020) 1144431 [arXiv:2101.03105] [INSPIRE].

[46] All-Sky-ASTROGAM collaboration, *All-Sky-ASTROGAM: a MeV Companion for Multimessenger Astrophysics*, *PoS* **ICRC2019** (2020) 579 [INSPIRE].

[47] A. Coogan, A. Moiseev, L. Morrison and S. Profumo, *Hunting for dark matter and new physics with GECCO*, *Phys. Rev. D* **107** (2023) 023022 [arXiv:2101.10370] [INSPIRE].

[48] A. Coogan, L. Morrison and S. Profumo, *Precision gamma-ray constraints for sub-GeV dark matter models*, *JCAP* **08** (2021) 044 [arXiv:2104.06168] [INSPIRE].

[49] J.A. Grayson et al., *BICEP3 performance overview and planned Keck Array upgrade*, in proceedings of the *SPIE Astronomical Telescopes + Instrumentation*, Edinburgh, U.K., 26 June–1 July 2016, *Proc. SPIE* **9914** (2016) 99140S [arXiv:1607.04668] [INSPIRE].

[50] SPT collaboration, *SPT-3G: A Multichroic Receiver for the South Pole Telescope*, *J. Low Temp. Phys.* **193** (2018) 1057 [INSPIRE].

[51] E. Calabrese et al., *Precision Epoch of Reionization studies with next-generation CMB experiments*, *JCAP* **08** (2014) 010 [arXiv:1406.4794] [INSPIRE].

[52] T. Essinger-Hileman et al., *CLASS: The Cosmology Large Angular Scale Surveyor*, in proceedings of the *SPIE Astronomical Telescopes + Instrumentation*, Montréal, Quebec, Canada, 22–27 June 2014, *Proc. SPIE* **9153** (2014) 91531I [arXiv:1408.4788] [INSPIRE].

[53] A. Suzuki et al., *The POLARBEAR-2 and the Simons Array Experiment*, *J. Low Temp. Phys.* **184** (2016) 805 [arXiv:1512.07299] [INSPIRE].

[54] P. Ade et al., *The Simons Observatory: Science goals and forecasts*, *JCAP* **02** (2019) 056 [arXiv:1808.07445] [INSPIRE].

[55] X. Chu, T. Hambye and M.H.G. Tytgat, *The Four Basic Ways of Creating Dark Matter Through a Portal*, *JCAP* **05** (2012) 034 [arXiv:1112.0493] [INSPIRE].

[56] T. Hambye, M.H.G. Tytgat, J. Vandecasteele and L. Vanderheyden, *Dark matter from dark photons: a taxonomy of dark matter production*, *Phys. Rev. D* **100** (2019) 095018 [arXiv:1908.09864] [INSPIRE].

[57] G. Krnjaic, *Probing Light Thermal Dark-Matter With a Higgs Portal Mediator*, *Phys. Rev. D* **94** (2016) 073009 [arXiv:1512.04119] [INSPIRE].

[58] V. Shtabovenko, R. Mertig and F. Orellana, *FeynCalc 9.3: New features and improvements*, *Comput. Phys. Commun.* **256** (2020) 107478 [arXiv:2001.04407] [INSPIRE].

[59] H. Ruegg and M. Ruiz-Altaba, *The Stueckelberg field*, *Int. J. Mod. Phys. A* **19** (2004) 3265 [hep-th/0304245] [INSPIRE].

JCAP03(2023)061